CFM: Language-aligned Concept Foundation Model for Vision

Kai Wittenmayer, Sukrut Rao†, Amin Parchami-Araghi†, Bernt Schiele, and Jonas Fischer

Max Planck Institute for Informatics, Saarland Informatics Campus
Saarbrücken, Germany
{kai.wittenmayer,sukrut.rao,amin.parchami}@mpi-inf.mpg.de
{schiele,jonas.fischer}@mpi-inf.mpg.de
† Equal contribution

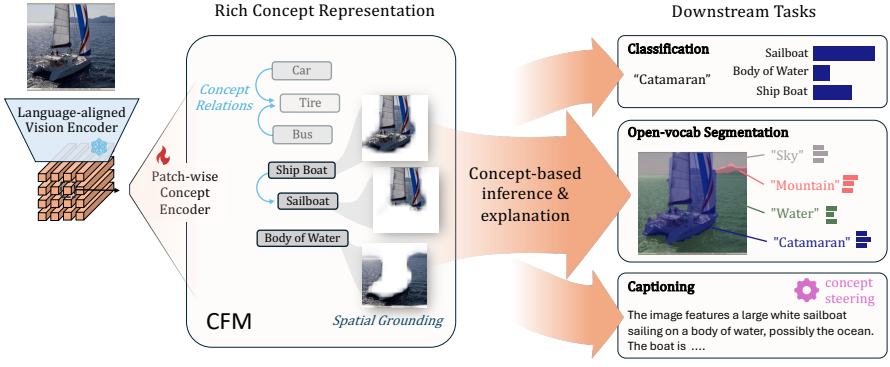

Fig. 1: CFM provides rich conceptual explanations for vision foundation model tasks. Our model provides a **hierarchical concept representation** (*e.g.* 'Sailboat' concept is a child of 'Ship Boat') with **local, spatially grounded** concepts that are automatically **named**. These concepts enable CFM to provide concept-based explanations for decision-making across vision tasks.

Abstract. Language-aligned vision foundation models perform strongly across diverse downstream tasks. Yet, their learned representations remain opaque, making interpreting their decision-making difficult. Recent work decompose these representations into human-interpretable concepts, but provide poor spatial grounding and are limited to image classification tasks. In this work, we propose CFM, a *language-aligned concept foundation model for vision* that provides fine-grained concepts, which are human-interpretable and spatially grounded in the input image. When paired with a foundation model with strong semantic representations, we get explanations for *any of its downstream tasks*. Examining local co-occurrence dependencies of concepts allows us to define concept relationships through which we improve concept naming and obtain richer explanations. On benchmark data, we show that CFM provides performance on classification, segmentation, and captioning that is competitive with opaque foundation models while providing fine-grained, high quality concept-based explanations. Code at https://github.com/kawi19/CFM.

1 Introduction

Language-aligned vision foundation models such as CLIP [56,68,81] serve as powerful feature extractors that perform strongly across tasks such as zero shot classification and open-vocabulary semantic segmentation. Such models also serve as vision encoders for large vision-language models [14, 36, 39] and generative models [82]. However, their representations are opaque, which hinders interpreting their decision-making. Interpretability is, however, key for human users, especially for safety critical applications, and explanations of decision-making can help to understand whether a model is right for the right reasons, increase trust in a model's prediction, investigate why a model failed, and steer it away from harmful outputs.

Concept Bottleneck Models have emerged as a widely successful approach to make model predictions more interpretable, with recent works [1,2,37,60,80] aiming to decompose representations of foundation models into human-interpretable concepts and achieve transparency at an unprecedented scale. However, extracted concepts are not often properly grounded in the input image [2, 60, 80], harming interpretability. Moreover, the existing approaches only provide a limited range of granularity of concepts [1, 2, 37, 60] and their spatial coverage [2, 60, 80], and inter-concept dependencies are not examined even when using hierarchical priors [80]. Textual concept labels, when assigned [2, 60], often stem from a limited vocabulary that is not tailored for large-scale and fine-grained conceptual diversity.

Besides these limitations of what concepts can capture, such models have not been used in the foundational setting, i.e. such concept representations have only been used for global tasks, typically classification. The lack of granular, well-grounded, and non-spurious concepts hinders application to local downstream tasks, such as segmentation or large vision-language model reasoning, whereas the underlying foundation model backbone would be capable of this.

In this work, we address these issues and propose CFM, a *language-aligned concept foundation model* that provides a unified concept representation applicable to local image regions, thus *enabling any downstream vision foundation model task previously not possible with concept-based explanations.* The discovered concepts are at varying granularities, spatially grounded in the image, and organized into hierarchies with explicit inter-concept dependencies. To achieve this we employ a semantically smoothened image encoding through DINOised CLIP features [72] and learn a sparse autoencoder with a matryoshka objective encouraging hierarchical structures of the concept representations [6, 80]. By learning the concept representation across local image regions (e.g., patches) we achieve spatially localized and human-aligned concepts from coarse to fine granularities and avoid spurious concepts common in the existing global concept bottlenecks. By examining co-occurrences of local concept activations we discover parent-child relationships between concepts that provide further insights into the learned semantics. We use these relations to refine concept labeling towards more accurate and meaningful textual concept labels. Our model enables interpretable decision-making across foundation model downstream tasks typical

for a language-aligned vision foundation models (see Fig. 1). Our contributions can be summarized as follows:

1. We propose a **concept foundation model** (CFM), lifting concept bottleneck models to language-aligned vision foundation models **applicable to any downstream task** beyond just image classification through unified local concept representations.
2. We show how to extract **explicit hierarchical relations** between foundational concepts that further improve the explanations of model decisions.
3. We propose an **improved concept labeling scheme** that explicitly takes these concept relationships into account.
4. Putting this together, CFM yields **human-interpretable concepts** at **diverse granularities** that are **spatially localized and well-grounded** in the input.

On benchmark data and through a human user study we show that in contrast to state-of-the-art, CFM yields concepts that are more quantitatively and qualitatively consistent, spatially more localized (Fig. 3), well organized into hierarchies (Fig. 4), and meaningfully named (Fig. 5). We further show that this added interpretability does not come with a degradation of performance across various downstream tasks. On image classification tasks CFM yields performances competitive with the state-of the-art concept-based and opaque baseline models (Fig. 6). On an image captioning task, CFM performs similar to its opaque backbone and enables steering (Fig. 7). CFM also enables interpretable open-vocabulary segmentation that is on par with opaque foundation model alternatives (Tab. 1, Fig. 8).

2 Related Work

Vision-language models (VLMs) such as CLIP [15, 30, 56], ALIGN [31], CoCa [77], and SigLIP [68,81] learn vision and text encoders that share a semantic latent space. Such models are typically trained on billions of paired image-text data through contrastive learning, yielding powerful but opaque language-aligned visual representations enabling tasks such as open-vocabulary classification and semantic segmentation. Our proposed method CFM is such a language-aligned vision encoder, but trained to provide a human-interpretable concept representation space.

Concept extraction methods aim to decompose learned representations from encoders into human-interpretable concepts through, e.g., clustering [25, 35, 48], non-negative matrix factorization [23] or a learned concept dictionary that is image-specific [2] or shared across images [37,53,60,80]. The latter, in particular, have been applied to VLMs, but (1) lack spatial grounding of concepts to the image [2, 60, 80], (2) learn a flat hierarchy of concepts [2, 37, 60], or (3) use a limited vocabulary and imprecise names [60]. Our CFM, in contrast, learns a rich set of spatially grounded concepts with explicit parent-child relationships

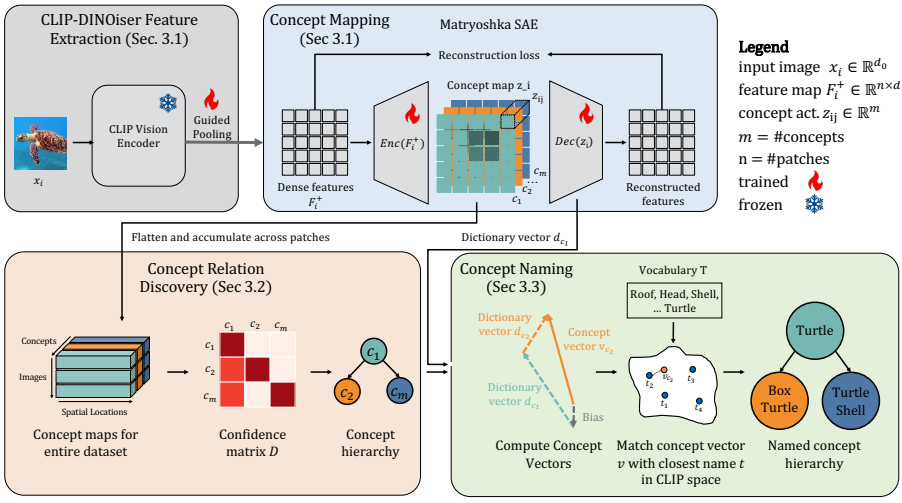

Fig. 2: Overview of CFM. We visualize our approach to represent human-interpretable, well localized, and consistent concepts of different granularities in a language-aligned vision foundation model. As backbone, we use pretrained CLIP-DINOiser [72] and extract concepts patch-wise by training a Matryoshka Sparse Autoencoder (SAE) without any supervision. From these learned concept representations, we discover concept relations through examining the co-occurrences of concepts within patches that allow more fine-grained interpretation of decision-making on downstream tasks. We further name the concepts with a Matryoshka-aware matching between concept representations and a large vocabulary of labels, taking the discovered concept relations into account.

that are named using a large fine-grained vocabulary taking such relationships into account, yielding a significantly more accurate, localized, and interpretable concept decomposition.

Sparse autoencoders (SAEs) [3,18] are models that aim to learn a dictionary of human-interpretable concepts from a latent space. These consist of an affine encoder and decoder that map features to a sparse high-dimensional space of concepts typically trained through a reconstruction and sparsity loss. SAEs have been shown a useful tool to understand large language models (LLMs) [3, 18], vision models [60, 80], and vision-language models [50]. Recent works suggested alternative sparsity objectives [5, 24, 57, 58] and architectural priors for concept hierarchies [6, 80] to improve SAE representations. Here, we combine the best of both worlds and use Matryoshka SAEs [6] with a BatchTopK objective [5] to extract high quality, localized, and hierarchical concepts.

Concept-based classification models such as concept bottleneck models (CBMs) [1,34,46,60,79] and visual prototype-based methods [12,21,45,75] learn concepts from a latent feature space to yield interpretable classification predictions. Where CBMs extract labeled, global concepts that are have shown to be often not correctly grounded in the image [29], prototypes are local visual

features that have to be investigated by a user to understand their conceptual meaning. Our approach bridges the gap between the two and helps construct inherently interpretable concepts that are labeled, can be global as well as local, and are well grounded in the input. Moreover, in the spirit of foundation models, CFM enables downstream tasks beyond just classification.

3 CFM: A Language-aligned Concept Foundation Model for Vision

To lift concept bottleneck models to be applicable to any vision foundation model downstream task we need accurate, spatially local concept representations. Here, we propose a language-aligned vision foundation model with explicit concept representations of local image regions, such as patches or pixels, that enable transparent, human-interpretable reasoning. In a nutshell, we learn a *local* mapping from dense, semantically smoothened image representations to a human-interpretable concept space. This concept space is encouraged to represent *concepts at varying levels of granularity*, so that we are able to discover locally consistent *concept hierarchies* describing part- or specification-relationships between concepts based on patch-wise concept co-occurrences (Fig. 2).

Specifically, as backbone we leverage CLIP-DINOised image embeddings [72], a CLIP architecture that encodes images such that semantically similar regions, informed through DINO [8], share similar representations. To map this latent CLIP encoding to meaningful concepts, we train a Sparse Autoencoder (SAE) on patch embeddings to learn *local* interpretable concept representations in an unsupervised manner at scale (Sec. 3.1). Through a Matryoshka objective, we further encourage to learn concepts at different levels of granularity. From these interpretable concept representations, we show how to extract relations between concepts that reflect both specifications as well as part-relations through an analysis of local co-occurrence patterns (Sec. 3.2). Finally, we extend the existing concept vocabularies used for labeling, show how to improve concept labeling by leveraging our discovered concept relationships, and show that an architecture-aware text encoding is necessary for accurate labels (Sec. 3.3).

3.1 From Global to Spatially Localized Concept Representations

We first extract human interpretable, spatially localized, and visually grounded concepts from latent features of the CLIP [56] vision encoder. We do this using sparse autoencoders (SAEs) [3], which we discuss first, and then describe our approach.

Background: Sparse Autoencoders (SAEs). Sparse autoencoders provide an efficient and unsupervised method to learn a concept mapping, crucial at the scale of foundation models. These consist of a light-weight linear layer encoder, $\pi^{enc} : \mathbb{R}^d \to \mathbb{R}^{d'}$ that describes an affine mapping from a d-dimensional input

space of CLIP features to a sparse representation where each dimension ideally encodes a single interpretable concept. An affine mapping $\pi^{dec} : \mathbb{R}^{d'} \to \mathbb{R}^d$ then maps back to the input space. The SAE is then trained through a reconstruction loss such that $\pi^{dec}\pi^{enc}(x) \approx x, \quad x \in \mathbb{R}^d$ and a sparsity regularization term on the encoder representations, typically via an ℓ_1 [3], TopK [24], or BatchTopK [5] constraint. Recent work [80] proposed Matryoshka SAEs to learn concepts across granularities. Specifically, let $C = [1 \dots m]$ be the index set for the m neurons in the SAE concept layer and $l_j \in C$ indices until which we define a matryoshka shell. Then

$$\mathcal{L}_{rec}(F_p) = \sum_j \left\| \pi^{dec}(\ \pi^{enc}(F_p)[1 : l_j]\ ) - F_p \right\|_2^2, \tag{1}$$

where F_p are the latent features for patch p given by the backbone model and $\pi^{enc}(F_p)[1 : l_j]$ sets all activations of neurons after index l_i to zero. Thus, each Matryoshka shell consisting of the first l_j neurons is trained to reconstruct the *full* latent features, which encourages that the smallest subset of neurons learns coarse, high-level information and higher-index neurons learn the *residual* fine-grained information on top of this coarse representation.

Extracting Semantic, Spatially Localized, and Grounded Concepts. While useful for learning concepts across granularities, concepts from such an SAE are not spatially localized, visually grounded to the input, and may not map well to human interpretable semantic features. To address this, we propose to use the following two approaches (Fig. 2, top).

Local Concept Extraction. Instead of encoding pooled visual features, we encode *each patch token* from the final layer of the CLIP vision encoder through the Matryoshka SAE, which helps encode spatially localized concepts. This also allows visual grounding, since concept strengths across spatial regions in the image can now be viewed as a heat map. We also use BatchTopK [5] instead of TopK for sparsity regularization as they provide more flexibility across samples.

DINOised CLIP Features. It has been shown that [86] fine-grained local representations can be extracted from CLIP by repurposing the patch token value vectors from the CLS attention as dense local embeddings. However, despite preserving a degree of spatial locality, they are noisy, which hurts concept extraction. To address this, we adopt the guided pooling approach introduced by CLIP-DINOiser [71], which smoothens the representations of semantically similar patches using affinity patterns of self-supervised features such as those from DINO [8] Intuitively, this pooling acts as a "voting system" that enforces consistency among semantically similar patches while "attenuating noisy features" [71]. For efficient inference via a single forward pass, a small 3×3 convolutional layer is trained on patch tokens to approximate the DINO affinity map. In our case, we DINOise the final layer patch tokens from CLIP before using them as inputs to the Matryoshka SAE; we refer to App. B for more details.

As compared to using pooled CLIP features, our approach helps obtain localized and better human-aligned concepts, since these DINOised local embeddings

Methods	Loc. ↑ Part	Loc. ↑ Stuff	Cons. ↑ Part	Cons. ↑ Stuff	Impur. ↓ Part	Impur. ↓ Stuff	C^2-Sc. ↑ IMN
SALF-CBM [1]	16.4	19.5	9.9	6.7	0.841	1.143	0.298
PatchSAE [37]	32.2	34.6	13.1	12.7	0.353	0.663	0.295
CFM	**44.3**	**44.5**	**15.3**	**13.1**	**0.333**	**0.539**	**0.405**

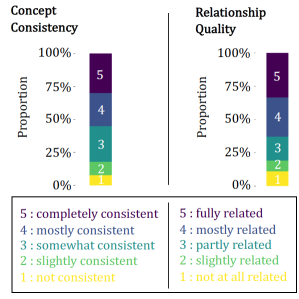

Fig. 3: CFM discovers consistent, well-grounded, and well-named concepts. ***Left:*** We quantitatively evaluate the consistency and grounding of our concepts using annotation-based and annotation-free metrics. Specifically, we compare against state-of-the-art concept extraction methods on part-annotated PartImageNet and COCO-Stuff, using metrics from [54], and measure localization of concepts, consistency of localization across images, and concept impurity across parts. We also evaluated C^2-Score [53] over ImageNet, which measures consistency of attributions independent of human annotations. ***Right:*** User study results on concept consistency (left) and relationship accuracy (right) for ∼1000 neurons each covered with 5 users in Amazon MTurk. We find our concepts to be highly consistent and with accurate relations.

are pooled from semantically coherent regions of the image which frequently correspond to meaningful object parts or localized visual attributes. Moreover, these extracted local embeddings remain well aligned with CLIP's language space, allowing them to still be directly associated with natural language descriptions through CLIP's pretrained text encoder.

3.2 Discovering Concept Relationships

The concept extraction procedure from Sec. 3.1 provides localized concepts at diverse granularities, but does not reveal inter-concept relationships. For example, a concept could be a specialization (*e.g.* 'leatherback turtle') or part (*e.g.* 'turtle shell') of a more general parent concept (*e.g.* 'turtle'). Identifying such relationships would help interpretability and allow for more effective steering of model decisions. Despite being trained to encode concepts at multiple granularities, extracting explicit relations from Matryoshka SAE concepts has so far not been explored. Other prior works rely on predefined concept hierarchies or leverage LLMs [52,66] to order concepts in a hierarchical manner, but these may not reflect the structure that emerges in the data or the model's reasoning process. In contrast, by discovering concept relations directly from data, we avoid mismatches between imposed taxonomies and the representations that the model actually uses.

To represent hierarchies, we identify pairs of parent and child concepts (Fig. 2, bottom left), where parents represent more general concepts and children capture more fine-grained or part-based specializations. In such a relation, the parent

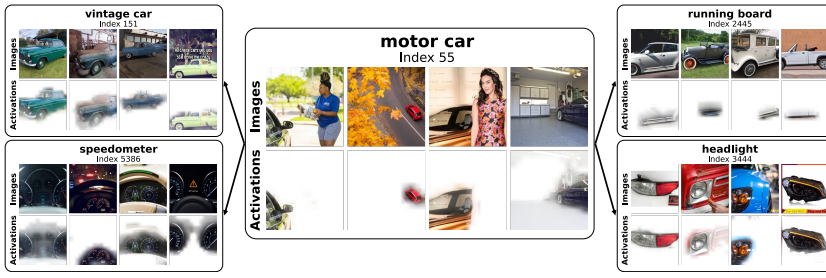

Fig. 4: A concept relationship subgraph. The parent concept, 'motor car', is shown in the center with children concepts arranged around it. For each concept, we provide the assigned label (top) and the top-4 most activating images (first row) along with their spatial localization (second row) based on concept activation strength per patch.

concept must also be active (*i.e.*, above a threshold, see App. B) whenever the specialized child concept is active. To identify such pairs, we construct a co-occurrence matrix $C \in [0,1]^{V \times V}$, such that C_{ij} denotes the weighted conditional probability of concept i being active given that concept j is active, *i.e.*

$$C_{ij} = \frac{\sum_{p:i,j \in B(p)} A_{ip}}{\sum_{p:j \in B(p)} A_{jp}} \tag{2}$$

where A_{ip} denotes the activation strength of concept i for patch p and $B(p)$ is the set of concepts active for patch p. We then use a threshold τ to prune weak associations, *i.e.*, a concept u is assigned to be a parent of concept v if $C_{uv} \geq \tau$, and construct our hierarchy.

For this to work, our design with *local, well-grounded* concepts is crucial as otherwise spatially unrelated concepts (e.g., *field* and *cow*) may incorrectly be assigned a relationship merely due to spurious correlations in their image-level activations. The discovered relations refine explanations through inter-concept dependencies and serve as a prior that allows to learn better concept labels discussed next.

3.3 Hierarchy-aware Concept Labeling

For human-understandable textual explanations of decision-making, prior work [60] assign labels for each concept neuron in an automated manner. They leverage the language-alignment of CLIP to assign labels l_i to a concept i, by finding the label v from a pre-defined vocabulary V whose CLIP text embeddings $\mathcal{T}(v)$ have the highest cosine similarity to the concept dictionary vector, given by the SAE decoder weights π_i^{dec}, *i.e.*

$$l_i = \text{argmin}_{v \in \mathcal{V}} \cos\left(\pi_i^{dec} + b, \mathcal{T}(v)\right), \tag{3}$$

where b is the SAE decoder bias. While this performs well for general concepts in the first Matryoshka group of the SAE, it fails for subsequent groups with fine-grained concepts since it does not take into account inter-concept dependencies

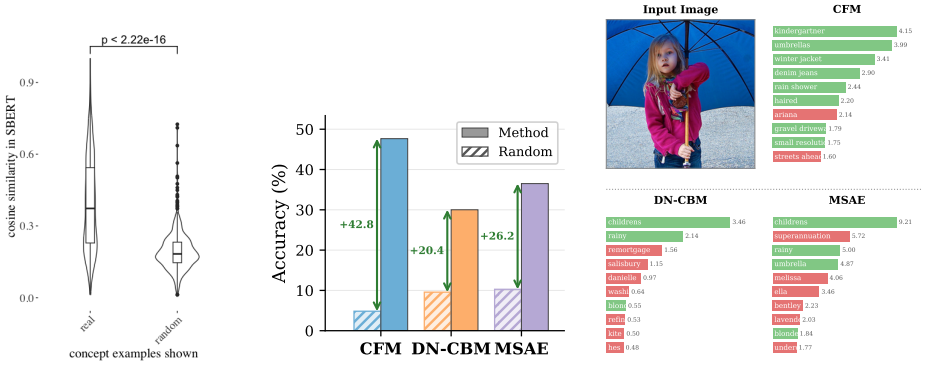

Fig. 5: CFM assigns concept names accurately. ***Left:*** We ask human annotators to provide a 1-2 word label for each concept, and compute cosine similarities with the concept name assigned by CFM using SBERT [61], and find a significant improvement over a random baseline. ***Middle:*** We use gpt-5-mini [65] as a judge to evaluate whether the top-10 concepts predicted by CFM and baselines are present in the image. CFM provides the most accurate concept names and has the biggest improvement over the random baseline. ***Right:*** A qualitative example of concept name accuracy. Green (red) indicate concepts present (absent) in the image as per the judge.

(see App. B). To account for this, we propose a hierarchy-aware naming scheme (Fig. 2, bottom right) that offsets child concept dictionary vectors with those of their parents, *i.e.*

$$l_j = \text{argmin}_{v \in \mathcal{V}} \cos\left(\left(\sum_{(i \to j) \in G} \pi_i^{dec}\right) + \pi_j^{dec} + b, \mathcal{T}(v)\right), \tag{4}$$

where $(i \to j)$ denotes a parent-child relationship in the extracted hierarchy G.

Putting all pieces together (Fig. 2), we obtain CFM, a concept foundation model which extracts language-aligned, spatially grounded, visually localized human-interpretable concepts across granularities for bringing interpretability to diverse downstream tasks.

4 Experimental Evaluation

We construct a CFM for a CLIP ViT-B/16 and use CC12M [10] to train the SAE with 8192 concepts and $K = 12$ concepts per patch for our main experiments. For more details including ablations on the number of concepts, see App. B. In Sec. 4.1, we evaluate the quality and interpretability of our extracted concepts, *i.e.* how localized, consistent, and pure they are via quantitative metrics and a human user study. We also evaluate accuracy of concept relationships and assigned names from CFM and compare them against baselines. Then, in Sec. 4.2, we evaluate the utility of CFM as a foundation model for diverse downstream

tasks. We first evaluate for image classification and show comparable performance to baselines, while enhancing interpretability. Next, we move to tasks that require local concept representations and show that CFM can be applied to yield meaningful image captions that are steerable through our concept layer. Finally, we use CFM for Open Vocabulary Segmentation (OVS) and show that it provides performance competitive with baselines while being the only method to provide explanations for the predicted segmentation.

4.1 Concept Quality and Interpretability

Locality, Consistency, Purity. We quantitatively evaluate concepts extracted from CFM (Sec. 3.1) for locality, consistency, and purity using metrics adapted from Pham *et al.* [54], on the part-annotated PartImagenet [26] and COCO-Stuff [7] datasets, and compare against state-of-the-art grounded concept extraction methods—SALF-CBM [1] and PatchSAE [37]. Specifically, to measure *locality*, we evaluate how well the concepts represent a human-annotated part by finding the maximal IoU between regions where the concept is active and the part annotation, across all parts. To measure *consistency*, *i.e.* how consistent parts map to the same concepts across images, we compute the maximal sum of part-specific IoUs across all parts. Lastly for the *impurity*, we evaluate how *semantically impure* a concept is by computing the per-concept entropy of normalized activation values across all parts. To avoid bias from dataset-annotated parts, we also compute the C^2-Score [53], which measures grounding consistency in DINOv2 [49] feature space, on ImageNet [19]. We find that CFM consistently outperforms (Fig. 3-left) all baselines across datasets and metrics, and in particular provides a significant improvement for locality. For more details, see App. A, and for comparisons with non-grounded baselines using post-hoc attribution methods, see App. C.

While relying on human-annotated part data for quantitative evaluation is an established benchmark in the field and provides a proxy for interpretability, ultimately we are interested in how well humans perceive and understand our discovered concepts. To do this, we conduct a large-scale user study via Amazon MTurk for concept consistency, with 1000 concepts and five annotators per task, which ask annotators to rate concepts on a five point scale. Each concept is shown via its top activating images and the regions it activates at. We show aggregated results in Fig. 3-right and provide detailed study design and results in App. A. We find that users rate concepts mostly or completely consistent for more than half of the shown concepts. More than 80% of annotators assign *at least* somewhat consistent, *i.e.* score 3 or higher. Taken together, we show that CFM **provides more interpretable and well-grounded concepts**.

Relationship Quality. We measure accuracy of our discovered hierarchy (Sec. 3.2) via a similar user study as above, where we show annotators pairs of two concepts and ask them to rate how well related they are. As shown in Fig. 3-right, we find that like with consistency, users rate concept hierarchies from CFM to

Model	Spatial Grounding	IMN	Places
Linear Probe	-	80.2	55.1
Zero Shot	-	68.6	41.2
LF-CBM [46]	✗	75.4	50.6
LaBo [76]	✗	78.9	-
CDM [51]	✗	79.3	52.6
DCLIP [42]	✗	68.0	40.3
DN-CBM [60]	✗	**79.5**	55.1
D-CBM [55]	✗	70.5	50.9
CF-CBM [52]	●	78.5	-
SALF-CBM [1]	✓	76.3	49.4
CFM	✓	78.9	**55.4**

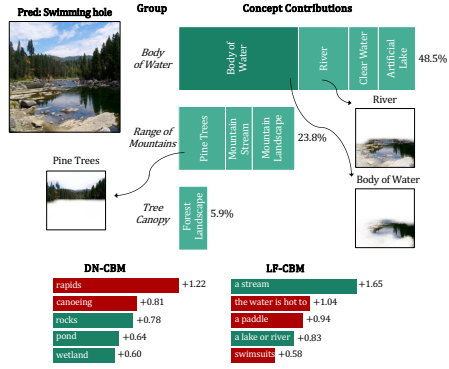

Fig. 6: CFM shows competitive classification performance while providing spatially grounded concepts. ***Left:*** We compare CFM with baselines on ImageNet (IMN) and Places365 (Places). "Spatial Grounding" indicates whether methods extract spatially grounded concepts (✓), partially local concepts (●), or global concepts only (✗). We show linear probe performance of CFM on max- and mean-pooled concept activations across patches. Baseline results taken from Prasse *et al.* [55], we retrained CFM on the same OpenAI-CLIP backbone, best method in **bold**. ***Right:*** For an image of the "Swimming hole" Class of Places365 we show explanations of CFM against existing method. For CFM, we provide the parent concept (dark green) and its contributing children (light green) with percentage of contribution and the spatial grounding of the top-3 most contributing concepts. In contrast to our work, existing methods (bottom) show spurious concepts.

be 'mostly' or 'fully' related for most pairs; for more details see App. A. We also show a qualitative example of discovered concept relations in Fig. 4, which shows visually well-grounded and meaningfully related concepts of varying granularities, and provide more examples in App. C. Overall, we show that **CFM organizes concepts into meaningful hierarchies** aiding interpretability.

Naming Accuracy. We perform two evaluations for the accuracy of concept names assigned by CFM (Sec. 3.3). First, we perform a user study, where we ask annotators to provide a 1-2 word description for a concept given top activating images with grounding. We then measure the cosine similarity between user-provided names and names assigned by CFM using SentenceBERT [61], and observe a strong statistically significant ($p < 2.22 \times 10^{-16}$ Wilcoxon rank-sum test) difference (Fig. 5-left) between our assigned names versus randomly drawn names using the set of concept names discovered by our method.

To evaluate its utility as a foundation model that can provide concepts, we also evaluate the accuracy of concept names found by CFM against baselines for images from the COCO [38] validation set. We use gpt-5-mini [65] as a judge, and ask it to decide whether each concept name from the top-10 concepts reported by each of the methods is present in the image. We find that CFM provides far more accurate concepts (Fig. 5-middle) as compared to the random baseline of randomly sampling concepts from the concept sets. This is also reflected

Metrics ↑	CLIP-DINO	CFM
CLIP-Sc [27]	0.72	0.72
RefCLIP-Sc [27]	0.73	0.72
Capture [20]	0.35	0.35

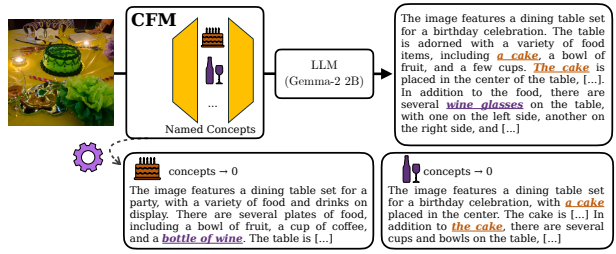

Fig. 7: CFM yields competitive and steerable captioning. ***Left:*** Captioning capabilities of CFM compared to its opaque backbone. ***Right:*** Through named concepts, CFM allows for concept-level intervention, steering the image captioning. For example, the 'cake' concept can be removed from the caption while preserving the 'drink' concept, and vice-versa. See also Apps. B and C for further examples and details.

qualitatively in Fig. 5-right. Overall, we show that **CFM assigns names that meaningfully align with human labeling** and more accurately describe what is in an image as compared to prior work.

4.2 Foundation Model Applications

Image Classification. We evaluate CFM for image classification on ImageNet [63] and Places365 [84] by training a linear classification head for each. We compare with recent CLIP ViT-B/16 based concept bottleneck models, *i.e.* LF-CBM [46], LaBo [76], CDM [51], DCLIP [42], DN-CBM [60], D-CBM [55], and CF-CBM [52]. We additionally include the ResNet-50 based SALF-CBM [1]. All baselines except SALF-CBM and CFM only provide image-level concepts. We find that **CFM yields competitive classification accuracies (Fig. 6-left) while also providing more interpretable and spatially grounded concepts (Fig. 6-right)**. Notably, all the baselines compared against are trained explicitly and only for classification, while CFM can do much more, which highlights the versatility concept foundation model.

Image Captioning. Next, we go beyond classification and show the utility of CFM's interpretable concept-based representation for image captioning. We follow the LLaVA setup [40], by learning a projection for spatial output tokens from CFM to a language model through an MLP adapter and fine-tune both the adapter and LLM (Gemma-2-2B Instruct [67]) captioner on CC12M DreamLIP Long captions [10, 83]. In Fig. 7-left we observe that CFM maintains captioning performance similar to the opaque, dense representation of the backbone, while providing an explicit concept representation. Importantly, **this representation can then be used to steer the captioning model**, as shown in Fig. 7-right.

Open-Vocabulary Segmentation (OVS). Finally, we use CFM for the challenging fine-grained task of semantic segmentation. Its language alignment allows

Table 1: CFM provides strong open-vocabulary semantic segmentation. We report mIoU between segmentations and annotated parts for each dataset considering evaluation with and without a 'background' prompt as discussed in App. A. We took baseline results from Wysoczańska *et al.* [72] and rerun (*) for inference consistency. First and second best method are **bold** and underlined, respectively.

Methods$^{+(\text{Variants/Extra Backbones})}$	No background prompt					w/ background			
	VOC20	C59	Stuff	City	ADE	Context	Object	VOC	Avg.
Build prototypes per class									
ReCo [64]	57.8	22.3	14.8	21.1	11.2	19.9	15.7	25.1	23.5
OVDiff [32]$^{+(\text{DINO \& SD})}$	81.7	33.7	-	-	14.9	30.1	34.8	67.1	-
*Text/image alignment **training** with captions*									
GroupViT [73]	79.7	23.4	15.3	11.1	9.2	18.7	27.5	50.4	29.4
ZeroSeg [13]	-	-	-	-	-	21.8	22.1	42.9	-
SegCLIP [41]	-	-	-	11.0	8.7	24.7	26.5	52.6	-
TCL [9]	77.5	30.3	19.6	23.1	14.9	24.3	30.4	51.2	33.9
CLIPpy [59]	-	-	-	-	13.5	-	32.0	52.2	-
OVSegmentor [74]	-	-	-	-	5.6	20.4	25.1	53.8	-
*Use **Frozen** CLIP*									
CLIP-DIY [71]$^{+(\text{DINO})}$	79.7	19.8	13.3	11.6	9.9	19.7	31.0	59.9	30.6
MaskCLIP [86]	61.8	25.6	17.6	25.0	14.3	22.9	16.4	32.9	27.1
MaskCLIP [86]$^{+(\text{ref}) [9]}$	71.9	27.4	18.6	23.0	14.9	24.0	21.6	41.3	30.3
CLIP-DINOiser* [72]	80.8	36.0	24.9	**39.4**	20.5	32.5	34.7	62.2	41.4
CLIP-DINOiser* [72]$^{+(\text{AnyUp}) [70]}$	81.6	37.2	**25.4**	39.1	20.9	33.8	**35.2**	**64.0**	**42.2**
*Use **Frozen** CLIP with **Interpretability***									
CFM	80.7	36.5	24.2	38.5	20.7	33.1	34.7	62.2	41.3
CFM$^{+(\text{AnyUp}) [70]}$	**81.8**	**37.6**	24.4	38.1	**21.1**	**34.3**	33.9	63.6	41.9

for open-vocabulary segmentation (OVS), *i.e.* can be used as is without expensive pixel-level data annotation limited to a fixed set of classes. To do this, we compute the cosine similarity between the embedding of each word in the segmentation vocabulary and the reconstructed *language aligned embedding* of the SAE. We consider two ways to obtain dense predictions. In one approach, we reconstruct patch-wise CLIP embeddings with the SAE and compute similarities to the vocabulary, after which predictions are upsampled to the pixel level using bilinear interpolation. Alternatively, we upsample the spatial concept activations directly to the pixel level using AnyUp [70] and reconstruct the CLIP embeddings with the SAE directly at pixel resolution before computing cosine similarities. In both cases, predictions are interpretable: the reconstructed CLIP embeddings are linear combinations of concepts through the SAE decoder, allowing either patch or pixel-level segmentation decision to be explained by a linear combination of concepts.

We compare against the reported performance of prototype-based [32, 64], segmentation-specific [9,41,59,62,73,74], as well as MaskCLIP and CLIP-DINOiser versions [72, 86] on a variety of benchmark datasets, including PASCAL VOC and VOC20 [22], PASCAL Context and Context59 [43], COCO Object [38] and Stuff [7]), Cityscapes [17], and ADE20K [85]. We report mIoU in Tab. 1 with and without a background prompt following established benchmarking protocols [72].

We observe that **CFM performs on par with the strongest opaque baselines**, *i.e.* CLIP-DINOiser and OVDiff. It also outperforms existing special-

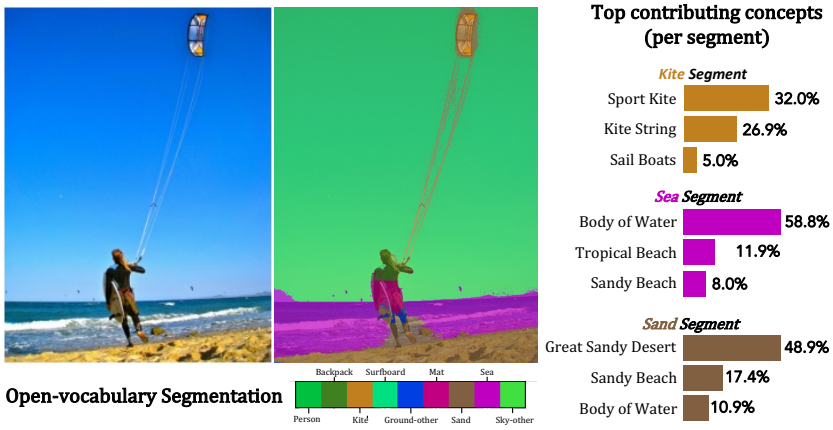

Fig. 8: Explainable Open-Vocabulary Segmentation. CFM$^{+(\text{AnyUp})}$ pixel-level open-vocabulary segmentation (left) with concept-based explanations for each segment (right).

ized architectures by a wide margin across datasets. In Fig. 8 we show a qualitative example of OVS on COCO-Stuff highlighting the interpretable downstream decision-making provided by CFM.

5 Discussion and Conclusion

We proposed CFM, a concept-based representation for a language-aligned vision encoder that represents spatially grounded and human-interpretable concepts of differing granularity. As such, CFM sets a new standard in the field of concept-based interpretability by providing meaningful, well-grounded concepts that are well-organized into hierarchies with meaningful concept names.

This work also comes with limitations. For instance, despite being significantly improved as compared CBMs and at foundation model scale (Fig. 5), there is still room for improvement for concept naming. There is also a plethora of evaluation strategies suggested for explanations, yet most of them are not directly applicable to concept-based explanations learned in an unsupervised manner. In this work, we focused on a set of interpretability metrics that cover a range of interpretability aspects and were established recently in the literature.

Building a highly diverse concept representation space by learning on corresponding large (web-scale) datasets would be an interesting direction for future work. Another highly interesting future application is enabling interpretable vision tokens to be used with large vision-language models (LVLMs) for tasks such as visual question answering (VQA).

In summary, CFM is **the first concept-based foundation model unlocking explanations for all its downstream vision tasks**.

Acknowledgements

Sukrut Rao and Bernt Schiele were funded in part by the Deutsche Forschungsgemeinschaft (DFG, German Research Foundation) – GRK 2853/1 "Neuroexplicit Models of Language, Vision, and Action" - project number 471607914.

References

1. Benou, I., Raviv, T.R.: Show and Tell: Visually Explainable Deep Neural Nets via Spatially-Aware Concept Bottleneck Models. In: CVPR. pp. 30063–30072 (2025)
2. Bhalla, U., Oesterling, A., Srinivas, S., Calmon, F.P., Lakkaraju, H.: Interpreting CLIP with Sparse Linear Concept Embeddings (SpLiCE). In: NeurIPS (2024)
3. Bricken, T., Templeton, A., Batson, J., Chen, B., Jermyn, A., Conerly, T., Turner, N., Anil, C., Denison, C., Askell, A., Lasenby, R., Wu, Y., Kravec, S., Schiefer, N., Maxwell, T., Joseph, N., Hatfield-Dodds, Z., Tamkin, A., Nguyen, K., McLean, B., Burke, J.E., Hume, T., Carter, S., Henighan, T., Olah, C.: Towards Monosemanticity: Decomposing Language Models With Dictionary Learning. Transformer Circuits Thread (2023)
4. Brysbaert, M., Warriner, A.B., Kuperman, V.: Concreteness Ratings for 40 Thousand Generally Known English Word Lemmas. Behavior Research Methods **46**(3), 904–911 (2014)
5. Bussmann, B., Leask, P., Nanda, N.: BatchTopK Sparse Autoencoders. arXiv preprint arXiv:2412.06410 (2024)
6. Bussmann, B., Nabeshima, N., Karvonen, A., Nanda, N.: Learning Multi-Level Features with Matryoshka Sparse Autoencoders. In: ICML (2025)
7. Caesar, H., Uijlings, J., Ferrari, V.: COCO-Stuff: Thing and Stuff Classes in Context. In: CVPR. pp. 1209–1218 (2018)
8. Caron, M., Touvron, H., Misra, I., Jégou, H., Mairal, J., Bojanowski, P., Joulin, A.: Emerging Properties in Self-Supervised Vision Transformers. In: ICCV (2021)
9. Cha, J., Mun, J., Roh, B.: Learning to Generate Text-Grounded Mask for Open-World Semantic Segmentation from Only Image-Text Pairs. In: CVPR. pp. 11165–11174 (2023)
10. Changpinyo, S., Sharma, P., Ding, N., Soricut, R.: Conceptual 12M: Pushing Web-Scale Image-Text Pre-Training to Recognize Long-Tail Visual Concepts. In: CVPR. pp. 3558–3568 (2021)
11. Chefer, H., Gur, S., Wolf, L.: Generic Attention-Model Explainability for Interpreting Bi-Modal and Encoder-Decoder Transformers. In: ICCV (2021)
12. Chen, C., Li, O., Tao, D., Barnett, A., Rudin, C., Su, J.K.: This Looks Like That: Deep Learning for Interpretable Image Recognition. In: NeurIPS. vol. 32 (2019)
13. Chen, J., Zhu, D., Qian, G., Ghanem, B., Yan, Z., Zhu, C., Xiao, F., Culatana, S.C., Elhoseiny, M.: Exploring Open-Vocabulary Semantic Segmentation from CLIP Vision Encoder Distillation Only. In: ICCV. pp. 699–710 (2023)
14. Chen, Z., Wu, J., Wang, W., Su, W., Chen, G., Xing, S., Zhong, M., Zhang, Q., Zhu, X., Lu, L., et al.: InternVL: Scaling up Vision Foundation Models and Aligning for Generic Visual-Linguistic Tasks. In: CVPR. pp. 24185–24198 (2024)
15. Cherti, M., Beaumont, R., Wightman, R., Wortsman, M., Ilharco, G., Gordon, C., Schuhmann, C., Schmidt, L., Jitsev, J.: Reproducible Scaling Laws for Contrastive Language-Image Learning. In: CVPR. pp. 2818–2829 (2023)

16. Contributors, M.: MMSegmentation: Openmmlab semantic segmentation toolbox and benchmark. https://github.com/open-mmlab/mmsegmentation (2020)
17. Cordts, M., Omran, M., Ramos, S., Rehfeld, T., Enzweiler, M., Benenson, R., Franke, U., Roth, S., Schiele, B.: The Cityscapes Dataset for Semantic Urban Scene Understanding. In: CVPR. pp. 3213–3223 (2016)
18. Cunningham, H., Ewart, A., Riggs, L., Huben, R., Sharkey, L.: Sparse Autoencoders Find Highly Interpretable Features in Language Models. In: ICLR (2024)
19. Deng, J., Dong, W., Socher, R., Li, L.J., Li, K., Fei-Fei, L.: ImageNet: A Large-Scale Hierarchical Image Database. In: CVPR. pp. 248–255 (2009)
20. Dong, H., Li, J., Wu, B., Wang, J., Zhang, Y., Guo, H.: Benchmarking and Improving Detail Image Caption. arXiv preprint arXiv:2405.19092 (2024)
21. Donnelly, J., Barnett, A.J., Chen, C.: Deformable ProtoPNet: An Interpretable Image Classifier using Deformable Prototypes. In: CVPR. pp. 10265–10275 (2022)
22. Everingham, M., Winn, J.: The PASCAL Visual Object Classes Challenge 2012 (VOC2012) Development Kit. Pattern Analysis, Statistical Modelling and Computational Learning, Tech. Rep **8**(5), 2–5 (2011)
23. Fel, T., Picard, A., Bethune, L., Boissin, T., Vigouroux, D., Colin, J., Cadène, R., Serre, T.: CRAFT: Concept Recursive Activation FacTorization for Explainability. In: CVPR. pp. 2711–2721 (2023)
24. Gao, L., la Tour, T.D., Tillman, H., Goh, G., Troll, R., Radford, A., Sutskever, I., Leike, J., Wu, J.: Scaling and Evaluating Sparse Autoencoders. In: ICLR (2025)
25. Ghorbani, A., Wexler, J., Zou, J.Y., Kim, B.: Towards Automatic Concept-Based Explanations. In: NeurIPS. vol. 32 (2019)
26. He, J., Yang, S., Yang, S., Kortylewski, A., Yuan, X., Chen, J.N., Liu, S., Yang, C., Yu, Q., Yuille, A.: PartImageNet: A Large, High-Quality Dataset of Parts. In: ECCV. pp. 128–145 (2022)
27. Hessel, J., Holtzman, A., Forbes, M., Bras, R.L., Choi, Y.: CLIPScore: a reference-free evaluation metric for image captioning. In: EMNLP (2021)
28. Hu, E.J., yelong shen, Wallis, P., Allen-Zhu, Z., Li, Y., Wang, S., Wang, L., Chen, W.: LoRA: Low-rank adaptation of large language models. In: ICLR (2022)
29. Huang, Q., Song, J., Hu, J., Zhang, H., Wang, Y., Song, M.: On the Concept Trustworthiness in Concept Bottleneck Models. In: AAAI. pp. 21161–21168 (2024)
30. Ilharco, G., Wortsman, M., Wightman, R., Gordon, C., Carlini, N., Taori, R., Dave, A., Shankar, V., Namkoong, H., Miller, J., Hajishirzi, H., Farhadi, A., Schmidt, L.: OpenCLIP (Jul 2021)
31. Jia, C., Yang, Y., Xia, Y., Chen, Y.T., Parekh, Z., Pham, H., Le, Q., Sung, Y.H., Li, Z., Duerig, T.: Scaling Up Visual and Vision-Language Representation Learning with Noisy Text Supervision. In: ICML. pp. 4904–4916 (2021)
32. Karazija, L., Laina, I., Vedaldi, A., Rupprecht, C.: Diffusion Models for Open-Vocabulary Segmentation. In: ECCV. pp. 299–317 (2024)
33. Kingma, D.P., Ba, J.: Adam: A Method for Stochastic Optimization. In: ICLR (2015)
34. Koh, P.W., Nguyen, T., Tang, Y.S., Mussmann, S., Pierson, E., Kim, B., Liang, P.: Concept Bottleneck Models. In: ICML. pp. 5338–5348 (2020)
35. Kowal, M., Wildes, R.P., Derpanis, K.G.: Visual Concept Connectome (VCC): Open World Concept Discovery and their Interlayer Connections in Deep Models. In: CVPR. pp. 10895–10905 (2024)
36. Li, B., Zhang, Y., Guo, D., Zhang, R., Li, F., Zhang, H., Zhang, K., Zhang, P., Li, Y., Liu, Z., Li, C.: LLaVA-OneVision: Easy Visual Task Transfer. TMLR (2025)
37. Lim, H., Choi, J., Choo, J., Schneider, S.: Sparse Autoencoders Reveal Selective Remapping of Visual Concepts During Adaptation. In: ICLR (2025)

38. Lin, T.Y., Maire, M., Belongie, S., Hays, J., Perona, P., Ramanan, D., Dollár, P., Zitnick, C.L.: Microsoft COCO: Common Objects in Context. In: ECCV. pp. 740–755 (2014)
39. Liu, H., Li, C., Li, Y., Lee, Y.J.: Improved Baselines with Visual Instruction Tuning. In: CVPR. pp. 26296–26306 (2024)
40. Liu, H., Li, C., Wu, Q., Lee, Y.J.: Visual instruction tuning. In: NeurIPS (2023)
41. Luo, H., Bao, J., Wu, Y., He, X., Li, T.: SegCLIP: Patch Aggregation with Learnable Centers for Open-Vocabulary Semantic Segmentation. In: ICML. pp. 23033–23044 (2023)
42. Menon, S., Vondrick, C.: Visual Classification via Description from Large Language Models. In: ICLR (2023)
43. Mottaghi, R., Chen, X., Liu, X., Cho, N.G., Lee, S.W., Fidler, S., Urtasun, R., Yuille, A.: The Role of Context for Object Detection and Semantic Segmentation in the Wild. In: CVPR. pp. 891–898 (2014)
44. Muraki, E.J., Abdalla, S., Brysbaert, M., Pexman, P.M.: Concreteness Ratings for 62,000 English Multiword Expressions. Behavior Research Methods **55**(5), 2522–2531 (2023)
45. Nauta, M., Schlötterer, J., Van Keulen, M., Seifert, C.: PIP-Net: Patch-based Intuitive Prototypes for Interpretable Image Classification. In: CVPR. pp. 2744–2753 (2023)
46. Oikarinen, T., Das, S., Nguyen, L.M., Weng, T.W.: Label-Free Concept Bottleneck Models. In: ICLR (2023)
47. Oikarinen, T., Weng, T.W.: CLIP-Dissect: Automatic Description of Neuron Representations in Deep Vision Networks. In: ICLR (2023)
48. O'Mahony, L., Andrearczyk, V., Müller, H., Graziani, M.: Disentangling Neuron Representations with Concept Vectors. In: CVPRW. pp. 3769–3774 (2023)
49. Oquab, M., Darcet, T., Moutakanni, T., Vo, H.V., Szafraniec, M., Khalidov, V., Fernandez, P., HAZIZA, D., Massa, F., El-Nouby, A., Assran, M., Ballas, N., Galuba, W., Howes, R., Huang, P.Y., Li, S.W., Misra, I., Rabbat, M., Sharma, V., Synnaeve, G., Xu, H., Jegou, H., Mairal, J., Labatut, P., Joulin, A., Bojanowski, P.: DINOv2: Learning Robust Visual Features without Supervision. TMLR (2024)
50. Pach, M., Karthik, S., Bouniot, Q., Belongie, S., Akata, Z.: Sparse Autoencoders Learn Monosemantic Features in Vision-Language Models. In: NeurIPS (2025)
51. Panousis, K.P., Ienco, D., Marcos, D.: Sparse Linear Concept Discovery Models. In: ICCVW. pp. 2767–2771 (2023)
52. Panousis, K.P., Ienco, D., Marcos, D.: Coarse-to-Fine Concept Bottleneck Models. In: NeurIPS. vol. 37, pp. 105171–105199 (2024)
53. Parchami-Araghi, A., Rao, S., Fischer, J., Schiele, B.: FaCT: Faithful Concept Traces for Explaining Neural Network Decisions. In: NeurIPS (2025)
54. Pham, N., Jesslen, A., Schiele, B., Kortylewski, A., Fischer, J.: Interpretable 3D Neural Object Volumes for Robust Conceptual Reasoning. In: ICLR (2026)
55. Prasse, K., Knab, P., Marton, S., Bartelt, C., Keuper, M.: DCBM: Data-Efficient Visual Concept Bottleneck Models. In: ICML (2025)
56. Radford, A., Kim, J.W., Hallacy, C., Ramesh, A., Goh, G., Agarwal, S., Sastry, G., Askell, A., Mishkin, P., Clark, J., et al.: Learning Transferable Visual Models from Natural Language Supervision. In: ICML. pp. 8748–8763 (2021)
57. Rajamanoharan, S., Conmy, A., Smith, L., Lieberum, T., Varma, V., Kramár, J., Shah, R., Nanda, N.: Improving Sparse Decomposition of Language Model Activations with Gated Sparse Autoencoders. In: NeurIPS (2024)

58. Rajamanoharan, S., Lieberum, T., Sonnerat, N., Conmy, A., Varma, V., Kramár, J., Nanda, N.: Jumping Ahead: Improving Reconstruction Fidelity with JumpReLU Sparse Autoencoders. arXiv preprint arXiv:2407.14435 (2024)
59. Ranasinghe, K., McKinzie, B., Ravi, S., Yang, Y., Toshev, A., Shlens, J.: Perceptual Grouping in Contrastive Vision-Language Models. In: ICCV. pp. 5571–5584 (2023)
60. Rao, S., Mahajan, S., Böhle, M., Schiele, B.: Discover-then-Name: Task-Agnostic Concept Bottlenecks via Automated Concept Discovery. In: ECCV (2024)
61. Reimers, N., Gurevych, I.: Sentence-BERT: Sentence Embeddings using Siamese BERT-Networks. In: EMNLP (2019)
62. Rewatbowornwong, P., Chatthee, N., Chuangsuwanich, E., Suwajanakorn, S.: Zero-Guidance Segmentation Using Zero Segment Labels. In: ICCV. pp. 1162–1172 (2023)
63. Russakovsky, O., Deng, J., Su, H., Krause, J., Satheesh, S., Ma, S., Huang, Z., Karpathy, A., Khosla, A., Bernstein, M., Berg, A.C., Fei-Fei, L.: ImageNet Large Scale Visual Recognition Challenge. IJCV **115**(3), 211–252 (2015)
64. Shin, G., Xie, W., Albanie, S.: ReCo: Retrieve and Co-segment for Zero-shot Transfer. NeurIPS **35**, 33754–33767 (2022)
65. Singh, A., Fry, A., Perelman, A., Tart, A., Ganesh, A., El-Kishky, A., McLaughlin, A., Low, A., Ostrow, A., Ananthram, A., et al.: OpenAI GPT-5 System Card. arXiv preprint arXiv:2601.03267 (2025)
66. Sun, A., Yuan, Y., Ma, P., Wang, S.: Eliminating Information Leakage in Hard Concept Bottleneck Models with Supervised, Hierarchical Concept Learning. arXiv preprint arXiv:2402.05945 (2024)
67. Team, G., Riviere, M., Pathak, S., Sessa, P.G., Hardin, C., Bhupatiraju, S., Hussenot, L., Mesnard, T., Shahriari, B., Ramé, A., Ferret, J., Liu, P., Tafti, P., Friesen, A., Casbon, M., Ramos, S., Kumar, R., Lan, C.L., Jerome, S., Tsitsulin, A., Vieillard, N., Stanczyk, P., Girgin, S., Momchev, N., Hoffman, M., Thakoor, S., Grill, J.B., Neyshabur, B., Bachem, O., Walton, A., Severyn, A., Parrish, A., Ahmad, A., Hutchison, A., Abdagic, A., Carl, A., Shen, A., Brock, A., Coenen, A., Laforge, A., Paterson, A., Bastian, B., Piot, B., Wu, B., Royal, B., Chen, C., Kumar, C., Perry, C., Welty, C., Choquette-Choo, C.A., Sinopalnikov, D., Weinberger, D., Vijaykumar, D., Rogozińska, D., Herbison, D., Bandy, E., Wang, E., Noland, E., Moreira, E., Senter, E., Eltyshev, E., Visin, F., Rasskin, G., Wei, G., Cameron, G., Martins, G., Hashemi, H., Klimczak-Plucińska, H., Batra, H., Dhand, H., Nardini, I., Mein, J., Zhou, J., Svensson, J., Stanway, J., Chan, J., Zhou, J.P., Carrasqueira, J., Iljazi, J., Becker, J., Fernandez, J., van Amersfoort, J., Gordon, J., Lipschultz, J., Newlan, J., yeong Ji, J., Mohamed, K., Badola, K., Black, K., Millican, K., McDonell, K., Nguyen, K., Sodhia, K., Greene, K., Sjoesund, L.L., Usui, L., Sifre, L., Heuermann, L., Lago, L., McNealus, L., Soares, L.B., Kilpatrick, L., Dixon, L., Martins, L., Reid, M., Singh, M., Iverson, M., Görner, M., Velloso, M., Wirth, M., Davidow, M., Miller, M., Rahtz, M., Watson, M., Risdal, M., Kazemi, M., Moynihan, M., Zhang, M., Kahng, M., Park, M., Rahman, M., Khatwani, M., Dao, N., Bardoliwalla, N., Devanathan, N., Dumai, N., Chauhan, N., Wahltinez, O., Botarda, P., Barnes, P., Barham, P., Michel, P., Jin, P., Georgiev, P., Culliton, P., Kuppala, P., Comanescu, R., Merhej, R., Jana, R., Rokni, R.A., Agarwal, R., Mullins, R., Saadat, S., Carthy, S.M., Cogan, S., Perrin, S., Arnold, S.M.R., Krause, S., Dai, S., Garg, S., Sheth, S., Ronstrom, S., Chan, S., Jordan, T., Yu, T., Eccles, T., Hennigan, T., Kocisky, T., Doshi, T., Jain, V., Yadav, V., Meshram, V., Dharmadhikari, V., Barkley, W., Wei, W., Ye, W., Han, W., Kwon, W., Xu, X., Shen, Z., Gong, Z., Wei, Z., Cotruta, V., Kirk, P., Rao,

A., Giang, M., Peran, L., Warkentin, T., Collins, E., Barral, J., Ghahramani, Z., Hadsell, R., Sculley, D., Banks, J., Dragan, A., Petrov, S., Vinyals, O., Dean, J., Hassabis, D., Kavukcuoglu, K., Farabet, C., Buchatskaya, E., Borgeaud, S., Fiedel, N., Joulin, A., Kenealy, K., Dadashi, R., Andreev, A.: Gemma 2: Improving Open Language Models at a Practical Size. arXiv preprint arXiv:2408.00118 (2024)
68. Tschannen, M., Gritsenko, A., Wang, X., Naeem, M.F., Alabdulmohsin, I., Parthasarathy, N., Evans, T., Beyer, L., Xia, Y., Mustafa, B., et al.: SigLIP 2: Multilingual Vision-Language Encoders with Improved Semantic Understanding, Localization, and Dense Features. arXiv preprint arXiv:2502.14786 (2025)
69. Turk, A.M.: Amazon Mechanical Turk, `https://www.mturk.com/`
70. Wimmer, T., Truong, P., Rakotosaona, M.J., Oechsle, M., Tombari, F., Schiele, B., Lenssen, J.E.: AnyUp: Universal Feature Upsampling. In: ICLR (2026)
71. Wysoczańska, M., Ramamonjisoa, M., Trzciński, T., Siméoni, O.: CLIP-DIY: CLIP Dense Inference Yields Open-Vocabulary Semantic Segmentation For-Free. In: WACV. pp. 1403–1413 (2024)
72. Wysoczańska, M., Siméoni, O., Ramamonjisoa, M., Bursuc, A., Trzciński, T., Pérez, P.: CLIP-DINOiser: Teaching CLIP a Few DINO Tricks for Open-Vocabulary Semantic Segmentation. In: ECCV. pp. 320–337 (2024)
73. Xu, J., De Mello, S., Liu, S., Byeon, W., Breuel, T., Kautz, J., Wang, X.: GroupViT: Semantic Segmentation Emerges from Text Supervision. In: CVPR. pp. 18134–18144 (2022)
74. Xu, J., Hou, J., Zhang, Y., Feng, R., Wang, Y., Qiao, Y., Xie, W.: Learning Open-Vocabulary Semantic Segmentation Models from Natural Language Supervision. In: CVPR. pp. 2935–2944 (2023)
75. Xue, M., Huang, Q., Zhang, H., Cheng, L., Song, J., Wu, M., Song, M.: ProtoPFormer: Concentrating on Prototypical Parts in Vision Transformers for Interpretable Image Recognition. In: IJCAI (2022)
76. Yang, Y., Panagopoulou, A., Zhou, S., Jin, D., Callison-Burch, C., Yatskar, M.: Language in a Bottle: Language Model Guided Concept Bottlenecks for Interpretable Image Classification. In: CVPR. pp. 19187–19197 (2023)
77. Yu, J., Wang, Z., Vasudevan, V., Yeung, L., Seyedhosseini, M., Wu, Y.: CoCa: Contrastive Captioners are Image-Text Foundation Models. TMLR (2022)
78. Yu, W., Wang, Q., Liu, C., Li, D., Hu, Q.: CoE: Chain-of-Explanation via Automatic Visual Concept Circuit Description and Polysemanticity Quantification. In: CVPR. pp. 4364–4374 (2025)
79. Yuksekgonul, M., Wang, M., Zou, J.: Post-hoc Concept Bottleneck Models. In: ICLR (2023)
80. Zaigrajew, V., Baniecki, H., Biecek, P.: Interpreting CLIP with Hierarchical Sparse Autoencoders. In: ICML (2025)
81. Zhai, X., Mustafa, B., Kolesnikov, A., Beyer, L.: Sigmoid Loss for Language Image Pre-Training. In: ICCV. pp. 11975–11986 (2023)
82. Zheng, B., Ma, N., Tong, S., Xie, S.: Diffusion Transformers with Representation Autoencoders. In: ICLR (2026)
83. Zheng, K., Zhang, Y., Wu, W., Lu, F., Ma, S., Jin, X., Chen, W., Shen, Y.: Dreamlip: Language-image pre-training with long captions. In: ECCV (2024)
84. Zhou, B., Lapedriza, A., Khosla, A., Oliva, A., Torralba, A.: Places: A 10 million Image Database for Scene Recognition. IEEE TPAMI (2017)
85. Zhou, B., Zhao, H., Puig, X., Xiao, T., Fidler, S., Barriuso, A., Torralba, A.: Semantic Understanding of Scenes through the ADE20k Dataset. IJCV **127**(3), 302–321 (2019)

86. Zhou, C., Loy, C.C., Dai, B.: Extract Free Dense Labels from CLIP. In: ECCV. pp. 696–712 (2022)

CFM: Language-aligned Concept Foundation Model for Vision

Appendix

In this supplement to our work on interpretable semantic hierarchies (CFM), we provide additional details on model training, experimental metrics, user study design and analysis, and additional qualitative results. In particular, Appendix A is dedicated to evaluation details, where we formally define the interpretability metrics reported in Fig. 3 in the main manuscript, discuss details of how we conducted the user study in Amazon MTurk, provide additional analysis of results stratified by concept activations frequency and results for concept naming quality, provide details about automated naming evaluation including prompts, and provide details about the open-vocabulary segmentation inference procedure.

In Appendix B, we provide all necessary technical details to reproduce our results, including formal definitions of CLIP-DINOiser, its training objective, how Matryoshka SAEs were trained including the choice of hyperparameters, and formal details on hierarchy discovery and concept naming used in CFM. Lastly we provide training details for the classification, image captioning tasks, and the open-vocabulary segmentation tasks.

In Appendix C, we provide additional results spanning all aspects of CFM, including concept relations, spatial grounding of concepts, and downstream tasks. We **highly encourage the reader to take a look at these results**. These are curated examples to show the diversity and granularity of concepts as well as concept hierarchies that CFM can find, but also to show the subtle limitations when it comes to naming fine-grained concepts. The following table of contents allows for fast access to the individual sections.

A Evaluation Details

A.1 Quantitative Interpretability Metrics

To quantitatively evaluate the locality of our discovered concepts, we compare CFM against three existing approaches: DN-CBM (data-driven global concepts), MSAE (data-driven global concepts), PatchSAE (data-driven local concepts), and SALF-CBM (predefined local concepts). Given the substantial differences in concept vocabularies, sparsity patterns, and spatial representations across these methods, we develop a comprehensive evaluation framework with five complementary metrics inspired by Pham *et al.* [54], adapted to enable fair comparison across diverse concept discovery approaches and diverse concept sets.

Locality Metric. This metric measures how well spatial activations of the concepts match human-annotated segments: Let $\mathbb{1}_c(i,j)$ and $\mathbb{1}_l(i,j)$ denote binary indicators of whether concept c or label l is active at pixel (i,j). For a concept c and label l on image x:

$$\mathrm{IoU}_{c,l}(x) = \frac{\sum_{i,j} \mathbb{1}_c(i,j) \cdot \mathbb{1}_l(i,j)}{\sum_{i,j} \mathbb{1}_{c,l}(i,j)}. \tag{A.1}$$

The overall Locality score is:

$$\text{Locality} = \frac{1}{|L_x|} \sum_{l \in L_x} \frac{1}{|I|} \sum_{x \in I} \max_{c \in C} \mathrm{IoU}_{c,l}(x). \tag{A.2}$$

where I is the set of images and L_x is the set of labels present in image x. For each image, we compute per human-annotated label the maximum IoU over all concepts and then average across images and labels.

Consistency Metric. This metric evaluates whether concepts reliably capture the same semantic regions across images:

$$\text{Consistency} = \frac{1}{|L|} \sum_{l \in L} \max_{c \in C} \frac{1}{|I_l^c|} \sum_{i \in I_l^c} \mathrm{IoU}_{c,l}(i), \tag{A.3}$$

where I_l^c is the set of images where both concept c and label l are present. For each concept-label pair, we compute the mean IoU across all images where both the concept and label are present, then take the maximum over concepts for each label.

Impurity Metric. This metric measures the spatial focus of concepts within single labels:

$$\text{Impurity} = \frac{1}{|C_{active}|} \sum_{c \in C_{active}} \frac{1}{|I_c|} \sum_{i \in I_c} H(p_i^c), \tag{A.4}$$

where C_{active} is the set of concepts that activate in at least 5 images for PartImageNet and 20 images for COCO-Stuff, I_c is the set of images where concept c is active, and $H(p_i^c)$ is the entropy of the normalized activation distribution of concept c across all labels (including background) in image i:

$$H(p_i^c) = -\sum_{l \in L \cup \{\text{bg}\}} p_i^{c,l} \log p_i^{c,l}, \tag{A.5}$$

where $p_i^{c,l} = \frac{\sum_{\text{pixels} \in S_i^l} B_i^c}{\sum_{\text{all pixels}} B_i^c}$. For each concept, we compute the entropy of its activations across all human-annotated labels (including background), then average over the images. For the final score we average over all concepts that activate at least in the specified number of images. Lower values indicate concepts that concentrate within specific semantic regions rather than spreading across multiple labels. Note that the metric is on a log scale.

A.2 User Study

To evaluate concept quality from a human perspective, we performed a large scale user study. In this section, we describe the setup and provide additional analyses of the results.

Study Setup. We conducted a study in Amazon Mechanical Turk [69] comprising three tasks: evaluating (1) concept consistency, (2) concept naming quality, and (3) concept relationship quality. Task 1 and task 2 consist of 1000 questions each, while task 3 contains 1100 questions. Each question is supposed to be labeled by five annotators. For each task, groups of 20 questions are created to form 'Human Intelligence Tasks' (HITs) in Amazon Mechanical Turk. A HIT is the smallest task unit an annotator can complete, *i.e.* for any task an annotator reads the instructions and completes 20 questions (and might optionally continue completing more HITs). To help annotation quality, we use annotators located in the US, with at least 10000 approved HITS, and with at least a 98% HIT approval rate. We pay annotators \$2.00 per completed HIT (*i.e.* \$0.10 per question), with an estimated time of five minutes for solving a HIT. All HITs inform annotators on how their responses will be used and require them to provide consent. In the following, we provide additional details about each task.

Task 1: Concept consistency. In this task we ask annotators to rate the consistency of concepts from CFM on a five-point scale. Each question consists of the top five activating images and corresponding concept locality maps for an CFM SAE latent (a concept). We call concept locality maps "focus regions" to ensure easier understanding for layman. We bin latents into five equi-height bins based on frequency of their activation across images, and sample uniformly from each bin. We sample 908 concepts and additionally create 92 'random' questions for control, *i.e.* questions where the 5 images and their focus regions are drawn iid from all SAE latents. For more details and an example, see Fig. A1.

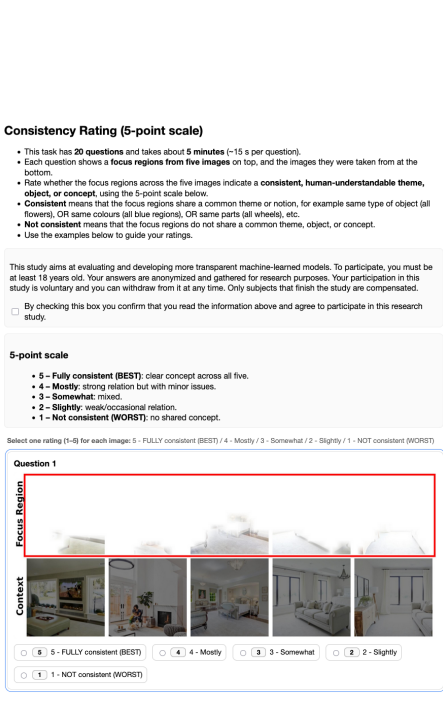

(a) *Top:* Task instructions. *Bottom:* A question in the task.

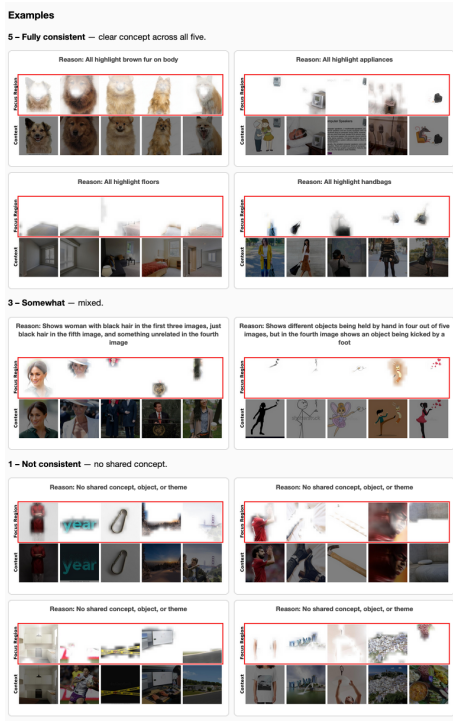

(b) Examples provided after the instructions to guide annotators.

Fig. A1: Task 1 instructions and an example question. See Sec. A.2 for details on the study setup.

Task 2: Concept naming quality. In this task we ask annotators to provide a one to two word label for an CFM concept. Each question consists of the top five activating images and corresponding concept locality maps for an CFM SAE latent. We follow the same binning based on activation frequency as above and sample equally from each bin. We sample 908 concepts and additionally create 92 'random' questions for control, *i.e.* questions where the 5 images and their focus regions are drawn iid from all SAE latents. If no name can be provided, annotators have the option to answer 'NA'. For more details and an example, see Fig. A2.

Task 3: Concept relationship quality. In this task we ask annotators to rate a given relationship between two concepts from CFM on a five-point scale, and we use this task to evaluate the quality of hierarchical relationships from CFM. Each question consists of the top three activating images and corresponding concept locality maps for two SAE latents from CFM. We bin latents into five bins based on frequency of their activation across images, and sample equally from each bin. We sample 990 concept pairs that correspond to edges from the

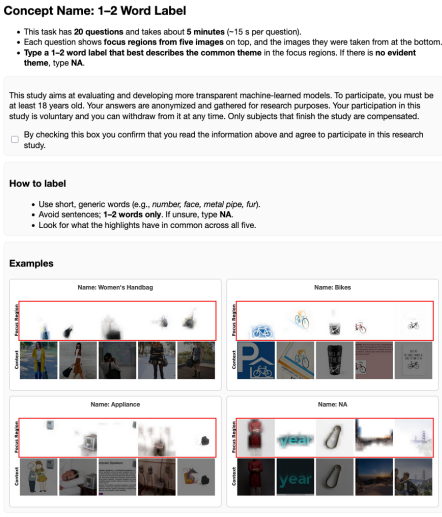

(a) Task instructions along with examples to guide annotators.

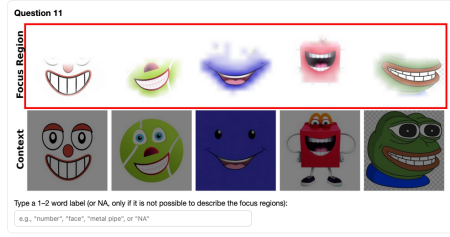

(b) A question in the task.

Fig. A2: Task 2 instructions and an example question. See Sec. A.2 for details on the study setup.

CFM concept hierarchies and additionally create 110 'random' relations across all concepts that do not have a real relation in our graph $\mathcal{G}$ for control. For more details and an example, see Fig. A3.

Quality Filtering. We apply three types of filtering to obtain consensual and higher quality results. For all tasks, we exclude those participants that did not answer the box asking for consent to being a participant. For task 1 and task 3, respectively, we filter out those participants that gave a score > 3 for one of the random control questions, as they likely did not understand the task or answered randomly. For task 2, we exclude those participants that gave NA as label for almost every question. This leaves us with scores of 152 unique participants for task 1, 107 for task 2, and 158 for task 3.

Statistics Stratified by Activation Frequency. To investigate how activation frequency of a concept, which is a reflection of its generality and correlates with the Matryoshka shells, impacts human interpretability, we investigate how stratification by activation frequency bins impacts study results. For both, task 1 and 2 (see Fig. A4), we observe that results look largely consistent across bins with slight improvements in scores for less frequently activated bins. In other words, we see a slight (negative) correlation between activation frequency and scores. This is to be expected, as frequently activated, general concepts activate on more diverse images, often capture more abstract or high-level concepts that

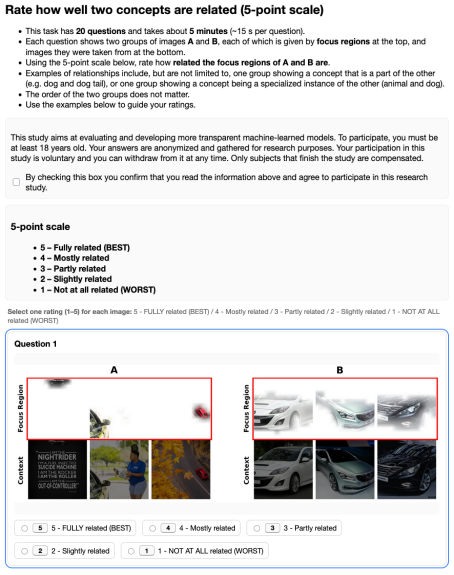

(a) *Top:* Task instructions. *Bottom:* A question in the task.

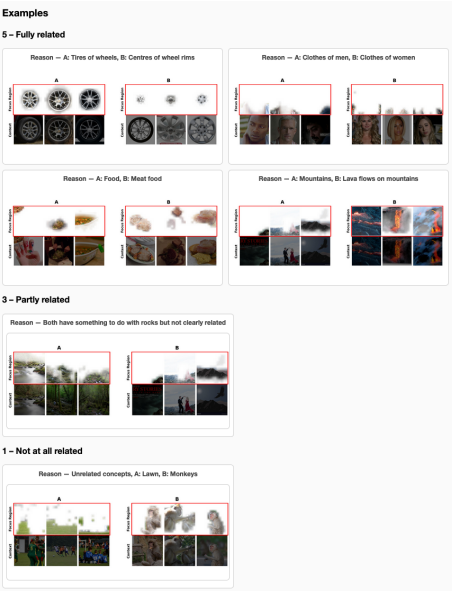

(b) Examples provided after the instructions to guide annotators.

Fig. A3: Task 3 instructions and an example question. See Sec. A.2 for details on the study setup.

are seemingly less consistent compared to the more specific concepts, given the larger variation in images. Similarly, it is harder to identify a clear and crisp label for a high-level concept compared to a highly specific one.

A.3 Naming Evaluation using an Automated Judge

As discussed in Sec. 4.1 and Fig. 5, we evaluate the accuracy of names assigned by CFM in comparison to baselines using an automated judge. Specifically, we compare against DN-CBM [60] and MSAE [80], since they both provide a concept decomposition that can be reconstructed to the original embedding, preserving the utility of the foundation model backbone. For each method, we obtain the top-10 concept names for each image from the MS COCO [38] validation set, and evaluate *whether the concept is present in the image*. For DN-CBM and MSAE, we additionally subtract the mean activation strength of each concept before ranking the top concepts per image, following the procedure used in those works.

Note that this evaluates concept presence unlike concept bottleneck evaluations (*e.g.* Fig. 6), which instead evaluate how much a concept contributed to a specific downstream classification task. We provide pairs of images and individual concepts to a gpt-5-mini [65] judge, and ask it to decide if that concept is present in the image. The prompt used is provided in Fig. A5.

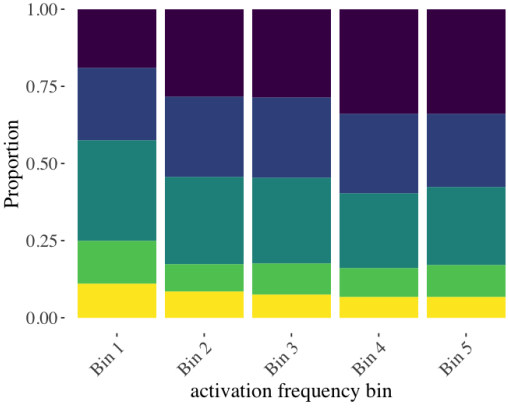

(a) Task 1 – Concept consistency per bin.

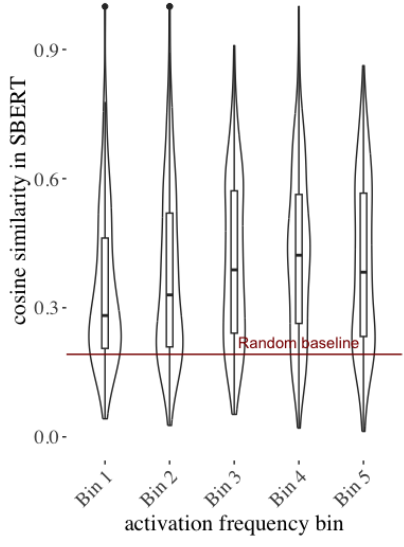

(b) Task 2 – Concept naming quality per bin.

Fig. A4: Additional User Study Results. We provide (a) concept naming quality, measured as average cosine similarity between SBERT embeddings of CFM concept naming and user-provided labels versus random names, p-value based on Wilcoxon rank-sum test, (b) concept consistency partitioned into concept activation frequency bins, with scores 1 (no consistency, yellow) to 5 (full consistency, purple) and (c) concept naming quality partitioned into concept activation frequency bins, red line indicates mean random similarity.

```
# Role
You are a visual evaluator whose task is to judge whether an image
contains a particular concept.

# Instructions
You will be given an:
- an image
- a text concept (a single word or short phrase)

Determine if there is anything in the image that looks like the concept.

Output:
- 1 if the image contains the concept.
- 0 otherwise.

Do not output anything else.
```

Fig. A5: Prompt provided to the automated judge. For details, see Sec. A.3.

Additionally, since each method uses a different concept set and a different vocabulary, we also evaluate with a random baseline for each method. For this, we sample ten concepts uniformly at random for each image from within the concept sets of each method. This helps better understand the true performance of each method, since using a concept set that has poor diversity but contains concepts that may be found in typical COCO classes could show a high accuracy by random chance. Nevertheless, concepts by CFM are rated the most accurate by a significant margin, with a 42.8 pp improvement over the random baseline (Fig. 5) as compared to 26.2pp for MSAE and 20.4pp for DN-CBM, respectively. For additional qualitative examples, see Sec. C.3.

A.4 Open-Vocabulary Segmentation Inference

We follow the standard MMSegmentation [16] sliding window inference protocol. While images are generally resized to a shorter side of 448 pixels and processed in 448×448 windows. For high-resolution datasets (Cityscapes, ADE20K, and COCO-Stuff) we pass images close to their original resolution. This prevents the loss of fine details and improves the performance of both CFM and CLIP-DINOiser [72]. Additionally, we utilize the background filtering strategy from CLIP-DINOiser to suppress non-foreground regions on datasets with a background prompt.

B Training Details

This section provides detailed training procedures for all components of CFM. We follow the notation established in the main paper (Sec. 3), recap the CLIP-DINOiser training, with a focus on the lightweight convolution, in Sec. B.1, discuss SAE training in Sec. B.2, hierarchy discovery in Sec. B.3, concept naming in Sec. B.4, classifier training in Sec. B.5, training for image captioning in Sec. B.6, open-vocabulary segmentation in Sec. B.7, and hyperparameter ablation in Sec. B.8.

B.1 CLIP-DINOiser Training

Following Wysoczańska *et al.* [72], we train a lightweight 3×3 convolutional layer $g : \mathbb{R}^d \to \mathbb{R}^{d'}$ with $d = 512$ and $d' = 64$ to approximate DINO affinity patterns from CLIP patch tokens.

Training objective. The convolution g is trained to predict binarized DINO [8] affinities. Given patch tokens X from the final CLIP layer L, we compute predicted affinities as follows:

$$A^{\phi} = \frac{g(\phi^L(X))}{\|g(\phi^L(X))\|} \otimes \left(\frac{g(\phi^L(X))}{\|g(\phi^L(X))\|} \right)^T. \tag{B.1}$$

The training loss is binary cross-entropy between A^{ϕ} and binarized DINO affinities $D = A^{\xi} > \gamma$:

$$\mathcal{L}^{\mathrm{C}} = \sum_{p=1}^{N} \left[D_p \log A_p^{\phi} + (1 - D_p) \log(1 - A_p^{\phi}) \right], \tag{B.2}$$

where $\gamma = 0.2$ is the binarization threshold.

Training setup. We train on 1,000 randomly sampled images from Imagenet [63] under learning rate of $5e-5$ with batch size of 16 for 100 epochs. The CLIP ViT-B/16 backbone ϕ and DINO ViT-B/16 remain frozen throughout training. For more details see Wysoczańska *et al.* [72].

B.2 Matryoshka SAE Training

We train hierarchical Matryoshka Sparse Autoencoders with BatchTopK sparsity [5] on DINOised patch features F^+ extracted as described in Sec. 3.1 of the main paper.

Architecture. The SAE consists of encoder $\pi : \mathbb{R}^d \to \mathbb{R}^m$ and decoder $\pi^{-1} : \mathbb{R}^m \to \mathbb{R}^d$ where $d = 512$ is the CLIP embedding dimension and $m = 8192$ is the number of concepts (expansion factor of 16).

For a patch embedding $F_p^+ \in \mathbb{R}^d$, the encoder computes pre-activation features:

$$z_{\text{pre}} = W_{\text{enc}}^T(F_p^+ - b_{\text{dec}}) + b_{\text{enc}} \ , \tag{B.3}$$

where $W_{\text{enc}} \in \mathbb{R}^{d \times m}$ are encoder weights, $b_{\text{enc}} \in \mathbb{R}^m$ is the encoder bias, and $b_{\text{dec}} \in \mathbb{R}^d$ is the decoder bias (shared with the decoder).

BatchTopK sparsity. Following Bussmann *et al.* [5], we apply batch-level top-k activation, which retains exactly $B \cdot k$ neurons across a batch of size B:

$$z = \pi(F_p^+) = \text{ReLU}(\text{BatchTopK}(z_{\text{pre}})) \tag{B.4}$$

where BatchTopK sets all but the top $B \cdot k$ pre-activations to zero across the entire batch. We use $k = 12$, meaning the SAE activates 12 concepts per patch on average.

Matryoshka structure. Following Sec. 3.1 of the main paper, we organize the $m = 8192$ concepts into six hierarchical groups with size ratios $[0.008, 0.03, 0.06, 0.12, 0.24, 0.543]$. Let $C = [1 \dots m]$ be the index set and $l_j \in C$ the index defining Matryoshka shell j. The reconstruction loss from the main paper is:

$$\mathcal{L}_{\text{rec}}(F_p^+) = \sum_j \cdot \left\| \pi^{-1}(\pi(F_p^+)[1 : l_j]) - F_p^+ \right\|_2^2 \ , \tag{B.5}$$

where $\pi(F_p)[1 : l_j]$ sets all activations after index l_j to zero.

Auxiliary loss for dead features. To recover neurons that haven't activated recently (last 10,000,000 samples), we add an auxiliary loss [24]:

$$\mathcal{L}_{\text{aux}} = \frac{\|r - W_{\text{dec}}^T z_{\text{dead}}\|_2^2}{\|r - \bar{r}\|_2^2} \ , \tag{B.6}$$

where $r = F_p^+ - \pi^{-1}(\pi(F_p))$ is the reconstruction residual, $\bar{r}$ is the batch-mean residual, and z_{dead} are activations for dead features only. Hence the total loss is

$$\mathcal{L}_{\text{total}} = \mathcal{L}_{\text{rec}} + \alpha_{\text{aux}} \cdot \mathcal{L}_{\text{aux}} \tag{B.7}$$

with $\alpha_{\text{aux}} = \frac{1}{32}$.

Training setup. We train on all DINOised patch embeddings extracted from CC12M [10]. Each image yields $N = 196$ patches (14×14 grid), providing approximately 2 billion training samples. We use Adam optimizer [33], with learning rate of $1e-4$. We set the batch size to 16,268 from 83 images and train for 3 epochs. We keep 10% of the patches as held-out validation set. Our training converges within 3 epochs with fraction of variance explained reaching approximately 73% and number of dead features dropping below 10.

B.3 Hierarchy Discovery

After SAE training, we discover concept relationships by analyzing patch-level co-occurrence patterns as described in Sec. 3.2 of the main paper. Note that during inference, we consider a concept j to be active if its activation exceeds an estimated threshold, which is derived to mimic the BatchTopK sparsity enforced during training.

Confidence matrix computation. For each concept pair (i, j), we compute the weighted conditional probability C_{ij} as defined in Eq. (2) using the SAE training dataset (CC12M [10]).

Graph construction. We construct the hierarchy graph $\mathcal{G} = (V, E)$ where $V = C$, i.e., vertices are concepts, and $(i, j) \in E$ if $C_{ij} \geq \tau$. This graph $\mathcal{G}$ defines our hierarchies, where each edge represents a parent to child (coarse to fine-grained) relationship. In this work we use $\tau = 0.75$. The threshold is an SAE-dependent hyperparameter determined via qualitative validation of the resulting hierarchies, selecting the lowest value that avoids spurious child relationships. We find that this value is stable and transfers well across different SAEs and datasets. In practice, $\mathcal{G}$ is typically a Directed Acyclic Graph (DAG) with potentially multiple parents per child.

B.4 Concept Naming

Following Sec. 3.3 of the main paper, we assign concept names using hierarchy-aware vector reconstruction.

Vector reconstruction. For fine-grained concepts in later Matryoshka groups, dictionary vectors π_i^{-1} alone are insufficient as they encode residuals from parent concepts (see Fig. B1). We reconstruct hierarchy-aware concept vectors:

$$v_{c_i} = b + \alpha \cdot w_{ii} \cdot \pi_i^{-1} + \sum_{a \in \mathcal{G}, a \to i} D_{ia} \cdot w_{ia} \cdot \pi_a^{-1}, \tag{B.8}$$

where:

- b is the SAE decoder bias b_{dec}
- π_i^{-1} is the dictionary vector (decoder weights for concept i)
- $a \to i$ denotes parent a of concept i in graph $\mathcal{G}$
- D_{ia} is the confidence from the co-occurrence matrix
- w_{ia} is the mean activation of concept a in the top-30 most activating patches of concept i
- $\alpha = 1.33$ is an empirically chosen coefficient to strengthen the concept's own direction in the embedding space

The coefficient $\alpha > 1$ ensures concept i's dictionary vector receives stronger weight than parent vectors, maintaining specificity while incorporating parent context.

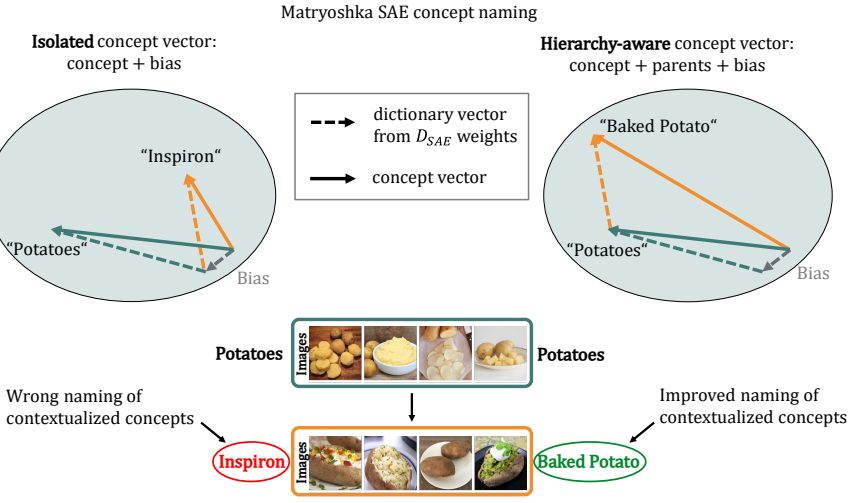

Fig. B1: Adapted concept vector reconstruction. In Matryoshka SAEs, dictionary vectors across different Matryoshka shells are residual by design. This means fine-grained concepts (e.g. "Baked Potato") are contextualized by coarser parent concept (e.g., "Potatoes"). Consequently, evaluating a fine-grained dictionary vector in isolation yields a misaligned representation (left), often resulting in erroneous textual labels such as "Inspiron" (bottom left). To resolve this, we reconstruct the concept vector by summing the target's dictionary vector with the vectors of all its parent concepts (right), which are identified as ancestors in our relationship graph (Sec. 3.2). This hierarchy-aware reconstruction is essential for assigning accurate, meaningful text labels to fine-grained concepts (bottom right).

Vocabulary matching. Given reconstructed vector v_{c_i}, we assign names as in Sec. 3.3:

$$l_i = \text{argmax}_{v \in V} \cos(v_{c_i}, \mathcal{T}(v)), \tag{B.9}$$

where $\mathcal{T}$ is the CLIP text encoder and V is our vocabulary.
As such, we get meaningful labels across concepts of different granularity. This assumes that the query vocabulary V is rich enough. We found that vocabularies used in concurrent works [60, 80] are often too limited for fine-grained concept labeling.

Vocabulary construction. To ensure comprehensive coverage, we construct our vocabulary by combining multiple resources. Concretely, our vocabulary includes (1) `Common words` as the 20k most frequent English words from [47], (2) a filtered 40k-word dataset from Brysbaert *et al.* [4], in which each word is annotated with a concreteness score between 1 (abstract) and 5 (highly concrete) and we retain only words with a mean concreteness above 2.5 as concreteness correlates strongly with imageability, (3) multi-word expressions from Muraki *et al.* [44], filtering with a concreteness threshold of 2.0, and (4) LAION expressions following the approach of Bhalla *et al.* [2], extracting the 40k most frequent uni-words

from LAION-400M, filtering NSFW captions using the given NSFW flag. Furthermore, we include the bi-words extracted by Bhalla *et al.* [2]. After gathering all resources, we merge them into a single comprehensive candidate vocabulary that balances coverage, concreteness, and fine-grained expressivity and provides a good resource for meaningful concept naming.

Vocabulary Templates. To improve labeling accuracy, we use sentence templates to encode the query vocabulary. However using the standard Zero-shot templates biases the labeling toward nouns, as CLIP's text encoder is sensitive to grammatical context. To allow concepts to be labeled by nouns, verbs, or adjectives, we introduce three distinct template sets, one for each part of speech. Each set contains ten abstract templates $\{\tau_k^{(p)}\}_{k=1}^{10}$, where $p \in \{\text{noun}, \text{verb}, \text{adj}\}$. Example templates include patterns such as "a photo of a {}" (noun), "a photo of someone {}" (verb), or "something that is {}" (adjective). We deliberately avoid overly specific templates to prevent unintentionally biasing the meaning of vocabulary items.

Given a vocabulary item $v \in V$, we generate its template-conditioned embeddings by applying the CLIP text encoder $\mathcal{T}$ to each templated prompt:

$$E_p(v) = \frac{1}{10} \sum_{k=1}^{10} \frac{\mathcal{T}\left(\tau_k^{(p)}(v)\right)}{\left\|\mathcal{T}\left(\tau_k^{(p)}(v)\right)\right\|_2}, \qquad p \in \{\text{noun}, \text{verb}, \text{adj}\}. \tag{B.10}$$

Each $E_p(v)$ is then normalized to unit length. For every concept vector v_{c_i}, we compute the cosine similarity to all template-conditioned embeddings:

$$s_i(v) = \max_{p \in \{\text{noun},\text{verb},\text{adj}\}} \cos(v_{c_i}, E_p(v)) \,. \tag{B.11}$$

Finally, we assign the vocabulary label that achieves the highest similarity:

$$l_i = \arg\max_{v \in V} s_i(v). \tag{B.12}$$

This template-based strategy enables each concept to select the grammatical form that best fits its semantics, yielding more accurate and fine-grained names than noun-only matching.

B.5 Probing for Classification

For downstream classification tasks, we train a linear probe on image-level concept activations while keeping all other components frozen (i.e., not fine-tuning).

Concept aggregation. We aggregate patch-level concept activations to image-level by combining max pooling and mean pooling:

$$\hat{c}_i^{\max} = \max_{p \in \{1,\dots,N\}} z_{i,p}, \qquad \hat{c}_i^{\text{mean}} = \frac{1}{N} \sum_{p=1}^{N} z_{i,p}, \tag{B.13}$$

and form the final image-level concept vector by concatenating both:

$$\hat{c}_i = [\hat{c}_i^{\max} | \hat{c}_i^{\text{mean}}], \tag{B.14}$$

where $z_{i,p} \in \mathbb{R}^m$ are the sparse concept activations given by our SAE concept mapping (see Eq.B.4) for patch p of image i, and $N = 196$ is the number of patches. We find that using only max-pooled concepts yields comparable performance: on ImageNet we match the reported accuracy, and on Places365, we observe only a 0.4% reduction.

Linear probe. We train a sparse linear classifier $h : \mathbb{R}^m \to \mathbb{R}^{|Y|}$ with ℓ_1 regularization:

$$\mathcal{L}_{\text{probe}} = \text{CE}(h(\hat{c}_i), y_i) + \lambda \|\omega\|_1, \tag{B.15}$$

where ω are the probe weights, y_i is the class label of image i, CE is cross-entropy loss, and λ controls the L1 sparsity loss.

Training setup. We use AdamW optimizer [33] with $\beta_1 = 0.9$, $\beta_2 = 0.999$ and set the learning rate to $1e-4$. We use batch size of 1024 and train for 100 epochs, taking the highest accuracy checkpoint. For the hyper-parameter search, we perform the following sweep over a held-out subset (10% of training data).

batch size $\in \{256, 512, 1024\}$, learning-rate $\in \{1e{-}3, 5e{-}4, 1e{-}4\}$,

$$\lambda_{\text{L1}} \in \{0.1, 1.0, 2.0, 4.0, 8.0\}.$$

All other components (CLIP encoder ϕ, DINOiser g, SAE π and π^{-1}) remain frozen.

Thresholded variant. For the thresholded variant reported in the main paper, we set patch activations below a learned threshold to zero before pooling. The threshold per concept is set to match the BatchTopK sparsity: we use the k-th largest activation value observed during SAE training, where $k = 12$.

B.6 Image Captioning

To explore the capabilities of CFM for downstream captioning task, we followed the setup of LLaVA training [40], mapping the dense output tokens to input words for a language model via an MLP adapter. Specifically, we took the 14×14 dense tokens after SAE reconstruction and used a 2-layer MLP to project them into 196 input words for an instruction-tuned Gemma-2 model [67] with 2 billion parameters.

Training. We trained our captioning setup (the adapter + the Gemma model) on CC12M DreamLIP synthetic captions [10, 83]. Specifically, for every image we randomly sampled one of the long synthetic captions from the dataset. We used an effective batch-size 96 for 30K steps. We split the training into two stages, where the first 13K steps only trained the MLP adapter under cosine learning-rate schedule (1e-2→1e-5) and in the second stage, the MLP and Gemma were jointly trained for 17K steps under fixed learning-rate of 1e-5. We used LoRA [28] (r=16, α=32) for updating Gemma parameters. Overall, we explored a lightweight captioning setup, with each training taking about 22 hours on a single H100 GPU. We note that we kept the backbone vision model, as well as the concept representation (SAE) frozen (i.e., no fine-tuning to this task).

We performed the above procedure both for CFM, as well as the same opaque backbone [72] without the concept representation of the SAE. The results from Fig. 7, which were demonstrated on unseen COCO [38] test-set (under Karpathy split) demonstrated that CFM achieves the same performance in terms of captioning, while additionally allowing for steering the generations through the named concepts Figs. C15 and 7.

B.7 Open-Vocabulary Segmentation

Patch-wise Concept Contributions. In our standard inference approach, the vision encoder processes the image into a grid of spatial patch tokens. Passing these tokens through the SAE yields a sparse concept activation vector for each individual patch. To perform segmentation, we reconstruct the dense CLIP embedding for each patch using the SAE decoder and compute its cosine similarity against the text embeddings of the target vocabulary.Because the reconstructed embedding is a linear combination of the active concepts, we can directly trace the model's decision back to individual concepts. We define the patch-wise concept contribution to a specific segmentation label as the product of the activation strength of the concept within that patch and the cosine similarity between the concept's dictionary vector (its corresponding weights in the SAE decoder) and the text embedding of the predicted label. This allows us to explicitly rank which concepts drove the segmentation prediction for any given patch.

Pixel-wise Concept Contributions. To achieve finer, pixel-perfect segmentation boundaries while preserving interpretability, we integrate AnyUp [70]. Rather than upsampling the final segmentation logits or the reconstructed dense

features, we apply the spatial upsampling directly to the sparse concept activations. This transforms the coarse grid of patch-level concept activations into a high-resolution map, providing a distinct concept activation vector for every single pixel in the image. Once we have these pixel-level concept activations, we pass them through the frozen SAE decoder to reconstruct the dense CLIP embedding at the pixel resolution. The segmentation prediction is then made by computing the cosine similarity between this pixel-level reconstructed embedding and the text vocabulary. Crucially, because the upsampling occurs purely within the concept space, the interpretability mechanism remains entirely intact at a much higher resolution. The pixel-wise concept contribution is computed exactly as it is in the patch-wise setting: by multiplying the upsampled pixel-level concept activation by the cosine similarity between the concept's dictionary vector and the predicted text label. This enables us to generate highly detailed explanation maps, where the decision for every individual pixel can be decomposed into its top contributing, human-understandable concepts.

B.8 Hyperparameter Ablation

In Tabs. B1 to B3, we ablate over various hyperparameters to validate our design choices.

Table B1: Downstream performance ablation over dictionary size (Classification and Segmentation). We evaluate classification and open-vocabulary segmentation performance across 4k, 8k, and 16k dictionary sizes. Note that the classification results in this table are with the OpenCLIP CLIP ViT-B/16 backbone, in contrast results in Fig. 6 are done with the OpenAI CLIP ViT-B/16 backbone for clear comparability with existing CBMs. The results demonstrate that an 8k dictionary size achieves the highest average segmentation performance while maintaining stable classification accuracy, justifying its selection as our default architecture.

Dict	Classification		Segmentation								
	IMN	Places	VOC20	C59	Stuff	City	ADE	Context	Object	VOC	Avg.
4k	78.2	55.5	80.7	36.6	24.1	38.5	20.5	33.2	33.1	62.1	41.1
8k	78.6	55.6	80.7	36.5	24.2	38.5	20.7	33.1	34.7	62.2	41.3
16k	78.6	56.0	80.0	36.2	24.3	37.6	20.5	32.8	33.7	61.6	40.8

Table B2: Interpretability ablation over dictionary size (Localization, Consistency, and Impurity). We assess the impact of dictionary size on concept spatial locality, consistency, and impurity. Notably, the results demonstrate that concept interpretability remains highly stable across different dictionary sizes.

Dictionary size	Locality↑		Consistency↑		Impurity↓	
	Part	Stuff	Part	Stuff	Part	Stuff
4k	43.9	44.2	15.8	12.5	0.34	0.54
8k	44.3	44.5	15.3	13.1	0.33	0.54
16k	44.6	44.7	15.7	13.6	0.34	0.54

Table B3: Dictionary metrics as in Zaigrajew *et al.* [80] on ImageNet. We find that concept sparsity helps produce highly interpretable concept-based explanations. Therefore, we select the sparsest possible configuration (BatchTopK of 12) that still maintains strong and stable SAE reconstruction.

Dict. Size	BatchTopK	L0 ↑	FVU ↓	CS ↑	CKNNA ↑	DO ↓	NDN ↓
8k	12	0.998	0.148	0.923	0.675	0.0020	6
4k	12	0.997	0.160	0.917	0.676	0.0034	4
16k	12	0.999	0.143	0.926	0.679	0.0040	472
8k	6	0.999	0.187	0.902	0.635	0.0042	1266
8k	32	0.995	0.108	0.945	0.731	0.0029	2
8k	64	0.991	0.078	0.961	0.713	0.0028	10
8k	128	0.982	0.043	0.979	0.493	0.0028	159
8k	256	0.966	0.012	0.994	0.095	0.0030	2453

C Additional Results

In this section we extend the results provided in the main paper. We begin with concept visualizations for different concept hierarchies in Sec. C.1, for different matryoshka fractions in Sec. C.2, and for accuracy of naming in Sec. C.3. We also provide further results on quantitative metrics in Secs. C.4 and C.5. We then further demonstrate the downstream interpretability and utility of CFM, with interpretable classification (Sec. C.6), interpretable open-vocabulary segmentation (Sec. C.7), and steerable captioning (Sec. C.8).

C.1 Concept Hierarchies

In Figs. C1 to C6 we provide more curated examples from our concept relation graph that show how hierarchies can deconstruct complex objects into their parts, that these hierarchies can have several levels of hierarchy and a concept can share multiple parents, that relationship can be based on concepts describing properties of another concept (e.g., material), and that relations can be abstract semantics (e.g., electricity, solar panel, and charging). With Fig. C5 we also show an example where relations are visually coherent, but naming can be limited, potentially because the concept vocabulary does not contain the relevant name or the text and image encoder of CLIP are not aligned for the specific fine-grained concept.

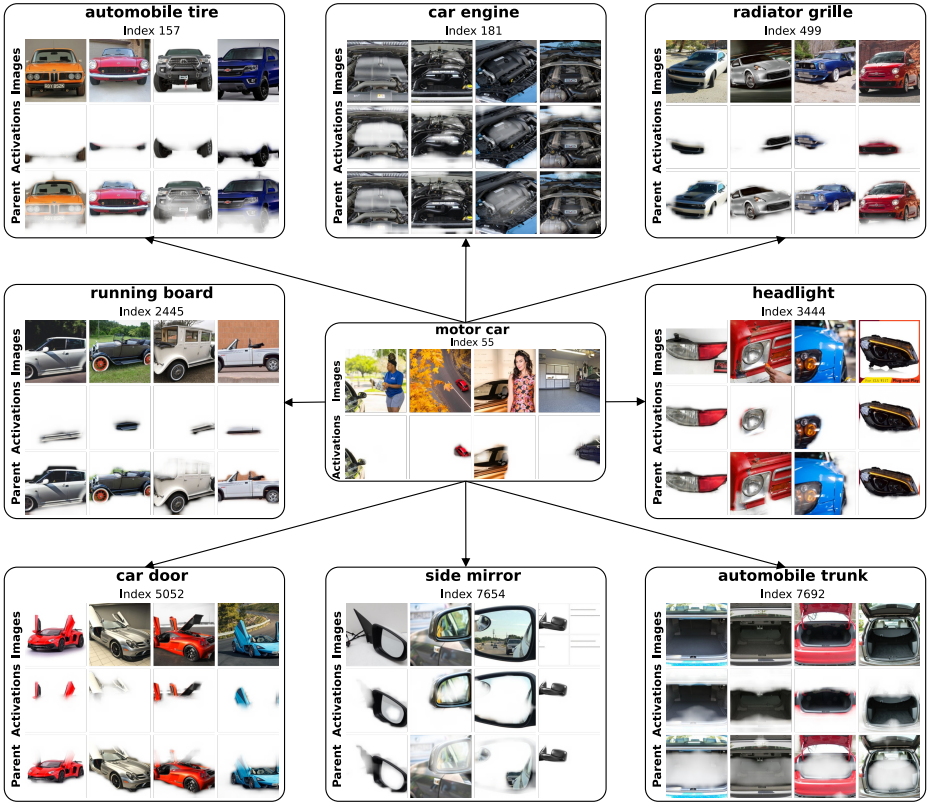

Fig. C1: Hierarchies deconstruct complex objects into to their parts. Here we show a subgraph of the 'motor car' hierarchy to illustrate that concept relationships can be formed as partonomies (part-based taxonomies). At the top of each concept visualization, we show the name and index of the concept, followed by a row of the top-activating images and their corresponding concept activation regions. For concepts with parents, we also show the parent activation on the same image below.

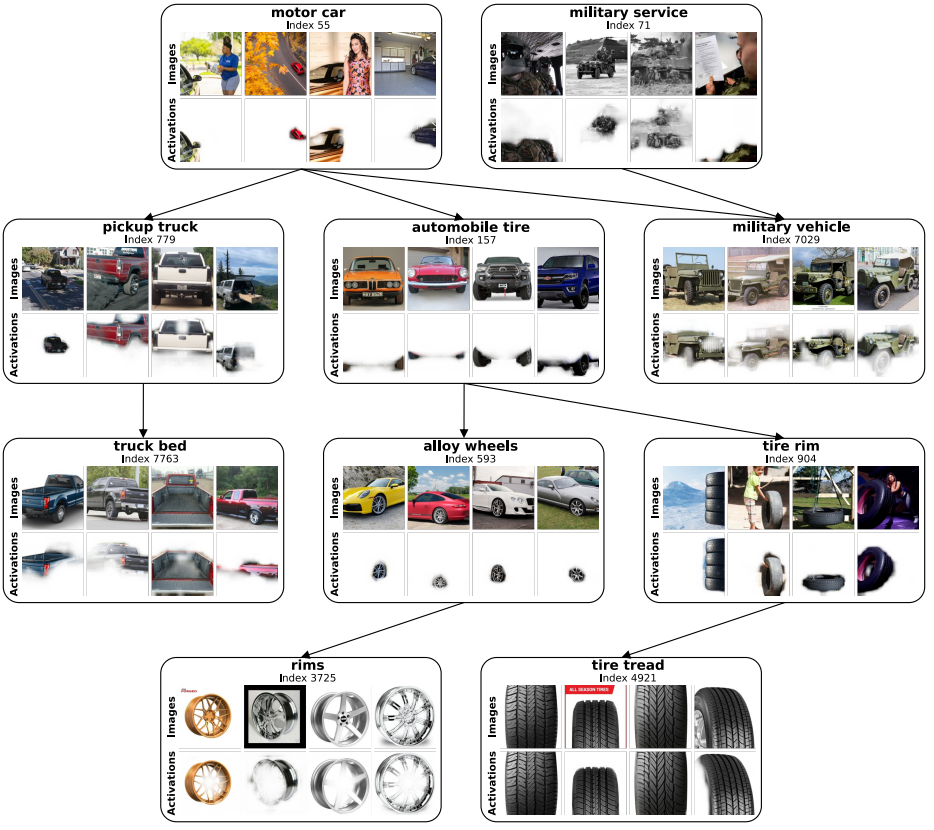

Fig. C2: Concept hierarchies have a DAG structure. We show a subgraph of the "motor car" hierarchy that shows the complexity of discovered hierarchies with several levels in the hierarchy and concepts having multiple parents (see 'military vehicle' with two parents 'motor car and 'military service'). Furthermore, the hierarchy also reveals progressively finer-grained concepts, such as 'alloy wheels' (third row) and the even finer subpart 'rim' (fourth row).

Fig. C3: Hierarchies can be semantically highly coherent. We show the entire "vineyard" hierarchy, i.e. the concept "vineyard" with all of its descendants and ancestors in the hierarchy graph $\mathcal{G}$. A hierarchy of acquired taste.

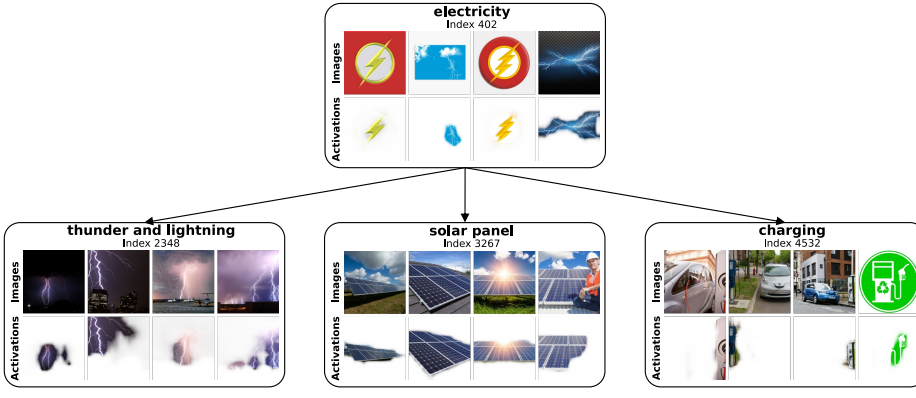

Fig. C4: Hierarchies can have abstract semantic relationships, without any common visual patterns. We show the full "electricity" hierarchy. Note that children like "solar panel" or "charging" do not share visual patterns with the top-activating examples of the parent "electricity", but instead are connected through an abstract semantic relationship.

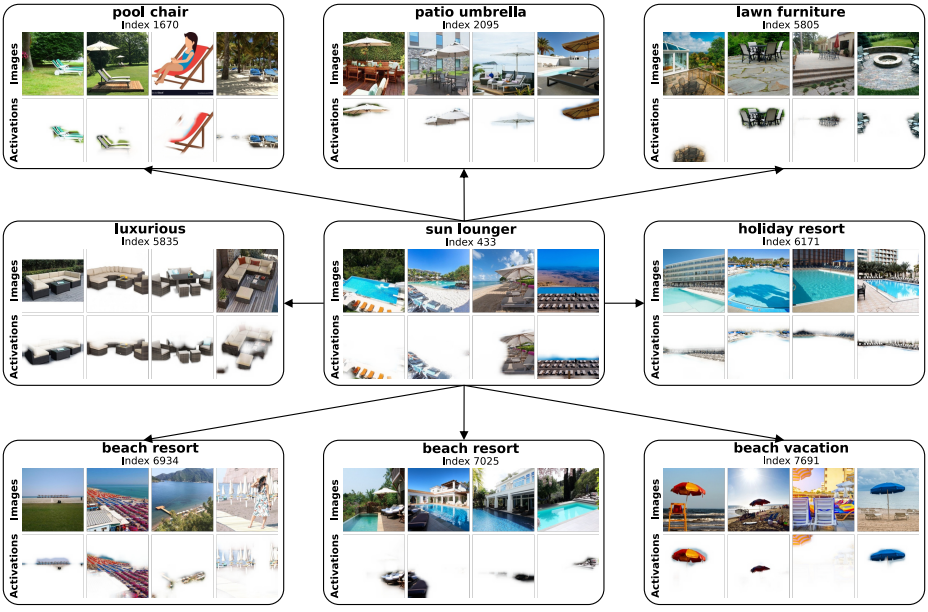

Fig. C5: Concept naming can be limited in the context of hierarchies. We show the entire "sun lounger" hierarchy with all of its descendents in the hierarchy graph $\mathcal{G}$. We observe that while the concept relations do make sense and concepts are spatially well grounded, concept naming is not ideal with multiple descendants receiving overly general names.

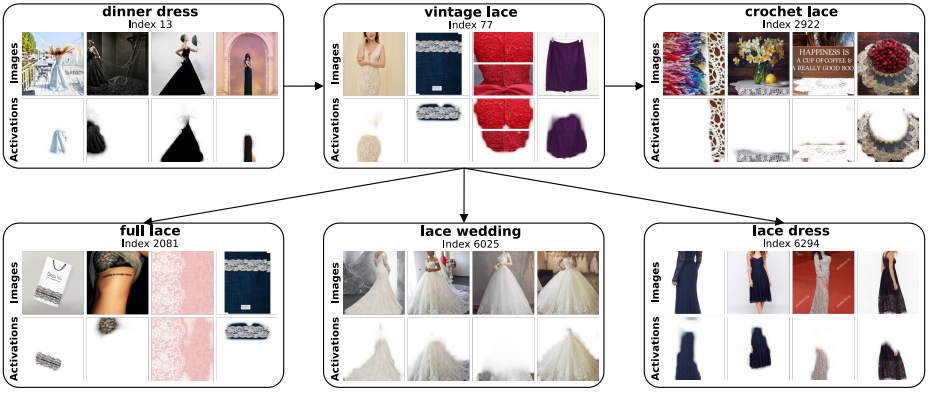

Fig. C6: Hierarchies can be based on material properties. We show the entire "vintage lace" hierarchy from the hierarchy graph $\mathcal{G}$. We find both specifications as well as sub-*material* relationships ("is made of").

C.2 Concept Consistency Visualization

We further show randomly sampled concepts for each Matryoshka group in Fig. C7 and observe that concepts are easy to understand, spatially well located, and correspond to frequent and less frequently used concepts.

Fig. C7: Randomly sampled Concepts per Matryoshka group. We show a random selection of concepts in each Matryoshka shell, defined by a range of neuron indices. By design of the Matryoshka training, the lower the range, the more "general" the information.

C.3 Concept Name Comparison

We provide additional examples of concepts extracted by CFM as compared to baselines in Fig. C8. This agrees with our observations in Sec. 4.1 and Fig. 5, where we show that CFM provides more accurate names as compared to baselines. For full experimental details, see Sec. A.3.

C.4 Polysemanticity Evaluation

To quantitatively evaluate the reduction in semantic entanglement, we utilize the Concept Polysemanticity Entropy (CPE) score introduced by Yu *et al.* [78]. The CPE metric operates on a logarithmic scale to measure concept polysemanticity, where lower scores indicate purer, more monosemantic representations. For this analysis, we compare the standard neurons from the patch tokens of the last transformer layer against our extracted CFM concepts. In the standard CPE evaluation protocol for convolutional architectures like ResNets, images are masked using the spatial neuron activations before being passed to the Vision-Language Model (VLM) to extract concept atoms. However, standard Vision Transformer (ViT) patch tokens generally exhibit poor spatial grounding, making this masked evaluation unreliable. Consequently, for ViTs, the standard baseline computes the CPE using entirely unmasked (non-local) images. For our extracted CFM concepts, we compute the CPE in both settings: with spatial masking (local) and without masking (non-local). Our results demonstrate that CFM successfully resolves polysemanticity. The standard ViT neurons yield a non-local CPE of 0.926. In contrast, our CFM concepts achieve a non-local CPE of 0.869, indicating that our formulation inherently reduces semantic ambiguity. Furthermore, when leveraging the strong spatial grounding of CFM to apply precise concept masks, the CPE drops even further to 0.814. This confirms that CFM provides disentangled concepts with accurate spatial localization.

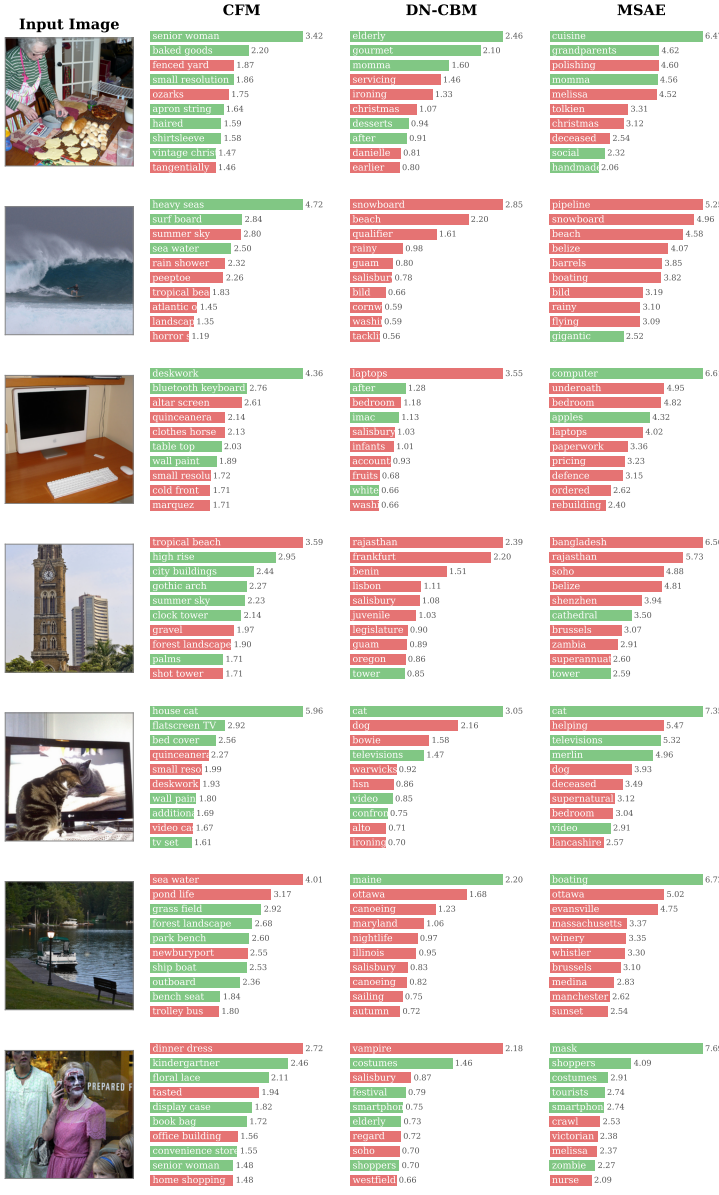

Fig. C8: Randomly sampled examples with extracted names. We show additional randomly sampled examples for the evaluation shown in Fig. 5. We find that on the whole, CFM provides more accurate names.

C.5 Concept Consistency Evaluation

We provide additional results for evaluation of concept consistency, localization, and impurity, as discussed in Sec. 4.1 and Fig. 3 in the main paper. Specifically, we compare across two additional baselines—MSAE [80] and DN-CBM [60], that do not directly provide image level grounding. Therefore, we use layer-wise relevance propagation (LRP) [11] to obtain pixel-level attributions, and evaluate with our localization, consistency, and impurity metrics, as shown in Tab. C1. We find that CFM outperforms both across metrics. We also compare across methods on the C^2-Score in Fig. C9, and find that CFM significantly outperforms most baselines, and is close to MSAE. This is despite the fact that unlike LRP, CFM does not require an additional backward pass.

Table C1: CFM discovers well-grounded and consistent concepts. We extend Fig. 3-left from the main paper and compare the inherent spatial grounding of CFM against global concept models (DN-CBM and MSAE), for which we apply a post-hoc attribution method [11]. We observe that CFM outperforms both across locality, consistency, and impurity metrics.

Methods	Loc. ↑		Cons. ↑		Impur. ↓	
	Part	Stuff	Part	Stuff	Part	Stuff
DN-CBM [60] + LRP [11]	18.7	17.9	9.3	5.7	0.761	1.235
MSAE [80] + LRP [11]	20.9	20.0	10.6	7.9	0.833	1.198
CFM	**44.3**	**44.5**	**15.3**	**13.1**	**0.333**	**0.539**

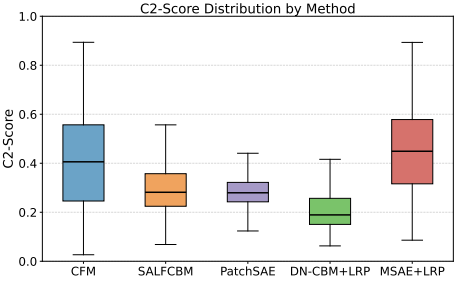

Fig. C9: We evaluate CFM against other baselines in terms of C^2-Score [53] and observe that it outperforms methods with inherent spatial concept activations (SALFCBM and PatchSAE). It also outperforms DN-CBM and performs similar to MSAE, all while not requiring a post-hoc attribution method (LRP) with additional backward passes.

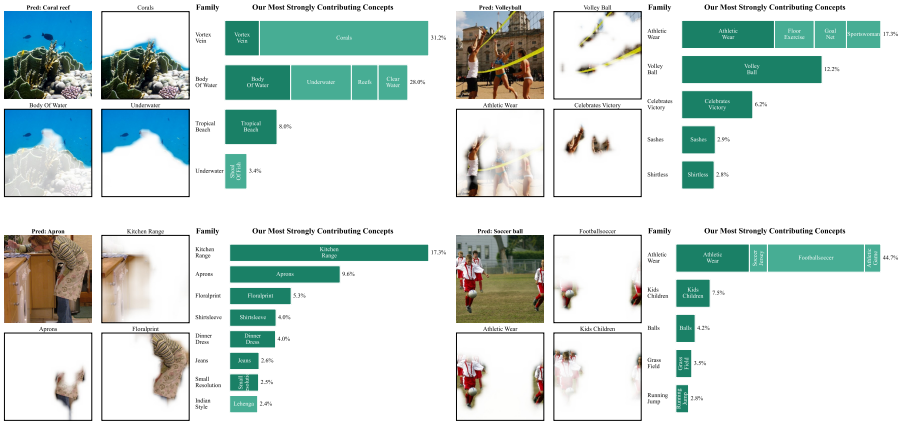

Fig. C10: Spatial grounding of concept-based explanations for Imagenet. We provide example images, their predicted class, along with fine-grained concept-based explanations showing contributions to prediction as bar plots, and spatial grounding in terms of per-patch concept activations.

C.6 Interpretable Classification

Here, we provide additional qualitative results explanations for classifications on ImageNet (Fig. C10) and Places365 (Fig. C11) and observe that explanations are rooted in spatially well-grounded fine-grained relevant concepts. Moreover, in contrast to many existing works, the top concepts cover a large fraction of the overall relevance for a classification, meaning the explanations are succinct, which is a natural consequence of using (batch) top-k SAE architectures.

C.7 Interpretable Open-Vocabulary Segmentation

In Fig. C12, we present randomly sampled qualitative explanations for the Pascal Context-59 dataset, specifically showcasing our method's pixel-level Open-Vocabulary Segmentation (OVS) prediction and explanation capabilities. Furthermore, Figs. C13 and C14 provide curated results demonstrating our patch-level OVS performance with interpretable explanations across PASCAL-VOC [22], COCO-Object [7], COCO-Stuff [7], and ADE20K [85]. Crucially, unlike existing approaches, our method allows us to explicitly decompose these segmentation logits into individual concept-wise contributions for any given text label, providing highly transparent decision rationales.

Fig. C11: Spatial grounding of concept-based explanations for Places365. We provide example images, their predicted class, along with fine-grained concept-based explanations showing contributions to prediction as bar plots, and spatial grounding in terms of per-patch concept activations. See also Fig. 8 of Rao *et al.* [60] for a comparison to existing methods.

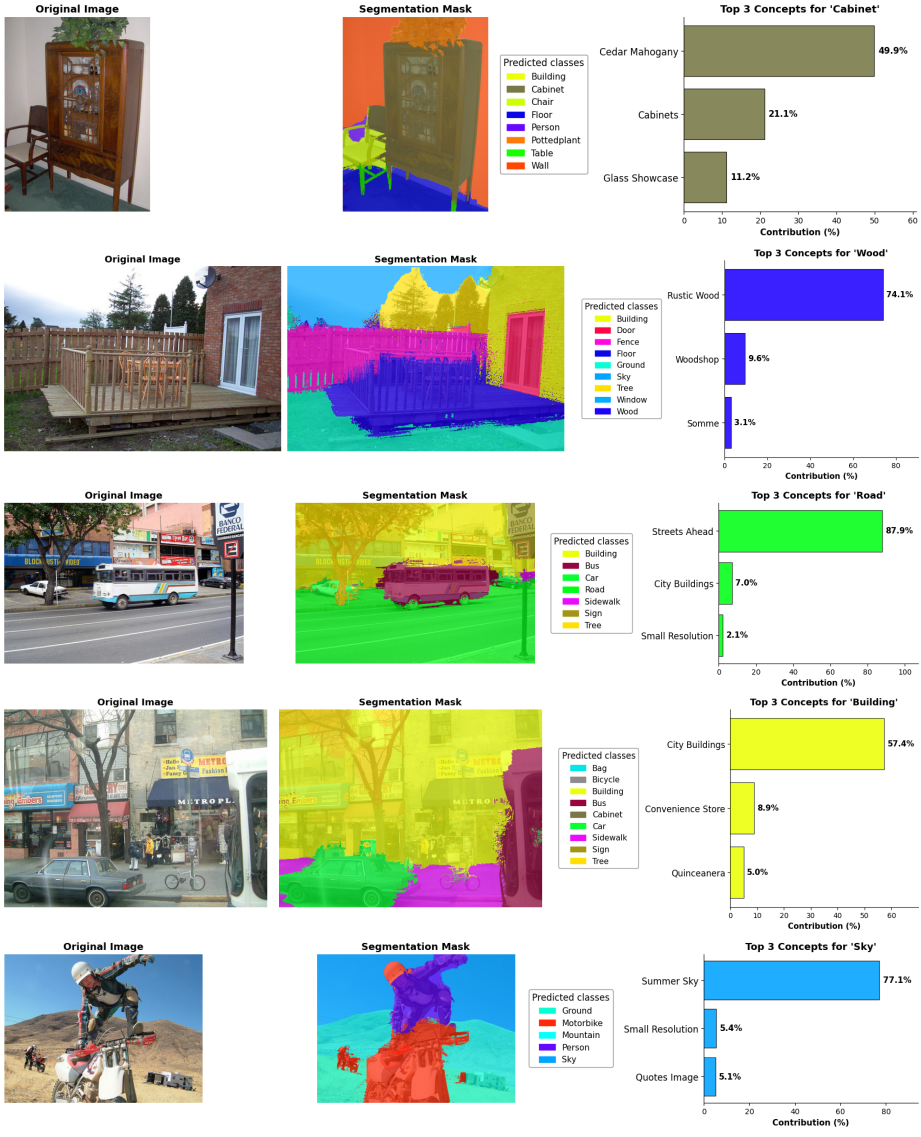

Fig. C12: CFM$^{+(\text{AnyUp})}$ provides high-quality, interpretable open-vocabulary segmentation at the pixel level. We show five randomly sampled scenes from the Pascal Context-59 dataset. For each example (row): Left: the original input image. Middle: the pixel-level segmentation mask produced by CFM. Right: a bar plot detailing the top contributing concepts for the largest predicted segment in the scene. The concept contributions are computed directly at the pixel level as the product of the spatially upsampled concept activation and its cosine similarity with the target label embedding. This illustrates how CFM yields highly transparent, fine-grained explanations for its dense predictions across diverse real-world scenes.

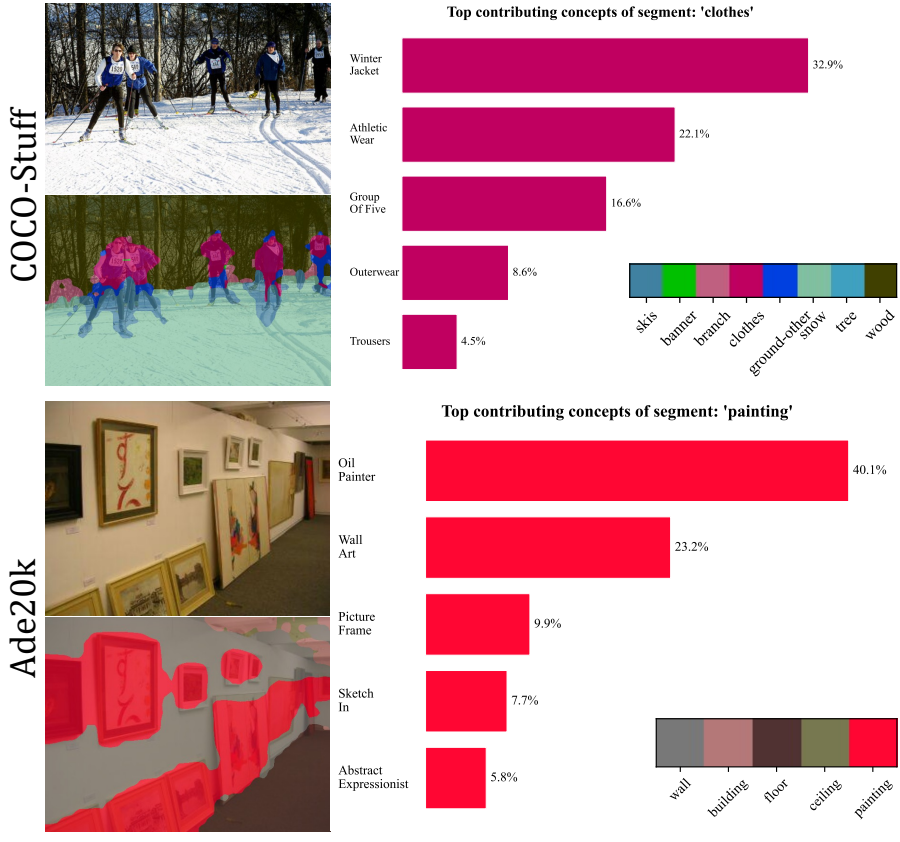

Fig. C13: CFM enables interpretable open-vocabulary segmentation. Top left: input image. Bottom left: segmentation produced by CFM when provided with the full set of dataset label names as text queries. Top right: bar plot showing the top contributing concepts for a selected segmentation label, where contribution is computed as the product of concept activation and its cosine similarity with the label embedding. Bottom right: all segmentation labels that the model identifies as present in the image. This illustrates how CFM produces both pixel-level predictions and transparent concept-level explanations of why each label is selected.

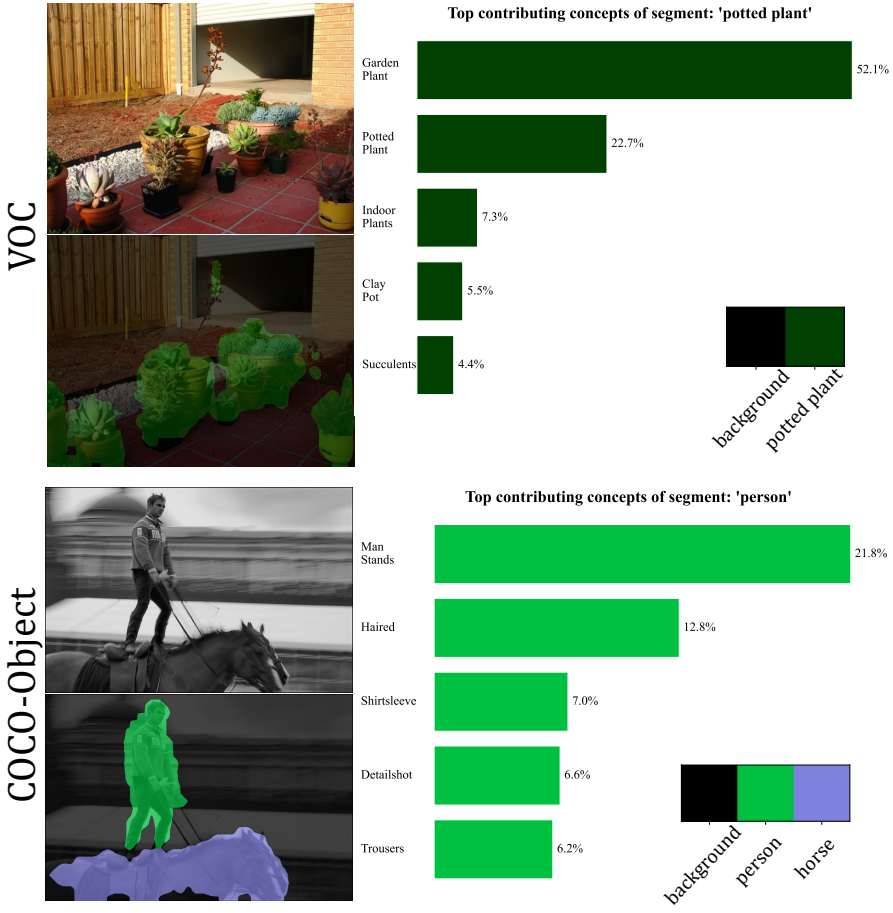

Fig. C14: CFM enables interpretable open-vocabulary segmentation with background removal. We demonstrate segmentation results when providing CFM with the full set of dataset label names together with an additional background prompt. The background label is used to filter out non-foreground regions, allowing the model to focus on semantically meaningful segments. As in the main results, CFM produces both pixel-level segmentations and concept-level explanations through contribution scores derived from concept activations and their cosine similarity with the corresponding label embeddings.

C.8 Steerable Captioning

We extend the qualitative results for captioning and steering shown in the main paper with additional samples. In Fig. C15, we show unseen test samples from the COCO dataset [38], and report the model captions before and after steering. The steered concepts were selected by asking Google-Gemini to search through activated concept names for relevant names.

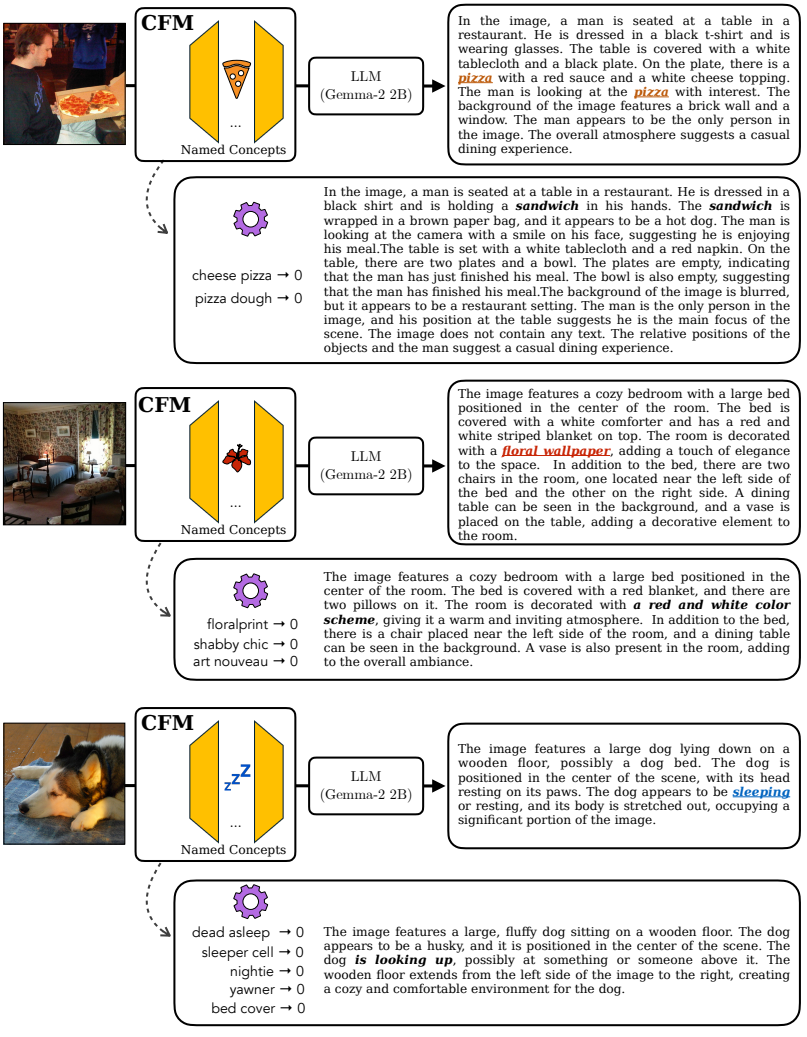

Fig. C15: Steering with CFM. In each example (major rows), we steer the output caption through intervention on the concept activations (left), *e.g.* on the first row the pizza-related concepts are disabled. For each case we asked Google-Gemini to find the relevant concepts among the activated names. We observe that the intervention is effective in steering the output caption, highlighting the utility of a concept-based bottleneck representation and the high quality of the concept naming.